Department for
Energy Security
& Net Zero

Projected wind-driven rain in the United Kingdom

Research Paper Number 2024/021

November 2024

Authors

Michael G. Sanderson, Michael Eastman, Jason A. Lowe

Met Office

Any enquiries regarding this publication should be sent to us at:
energyresearch@energysecurity.gov.uk

Contents

Executive Summary

Wind driven rain is rain that falls on vertical surfaces and elements of a building (walls, chimneys, doors, windows, etc.) and can lead to ingress of water and moisture damage to building fabric. This makes the likelihood, magnitude, and frequency of wind driven rain important considerations in the design of buildings and insulation of walls, for example where retrofitting cavity walls with insulation. While there is existing guidance based on historical wind driven rain data, changes to future wind driven rain are an evidence gap addressed by this study. This study has used the latest UK Climate Projections (UKCP18) to model changes in projected wind driven rain for 2°C and 4°C warming scenarios.

Wind driven rain is addressed in Approved Document C of the Building Regulations. This includes a map of wind-driven rain zones for the country, with guidance dependant on the wind-driven rain zone a building is in. The wind driven rain zones in Approved Document C are based on a dataset from historical weather station observations. The Technical Report for the 3rd Climate Change Risk Assessment noted under “Risks to Building Fabric” that uncertainty around future changes to wind driven rain required further investigation.

This study used high resolution data at an hourly timescale from UKCP18 Climate Projections to model projected wind driven rain under 2°C and 4°C warming scenarios. Validation and bias correction were carried out using observed weather data for present day modelled values. This showed reasonable consistency in observed wind driven rain and wind driven rain modelled from the climate projections, providing a degree of confidence in the modelled values for future scenarios.

Key findings from this study include:

1. Changes in projected wind driven rain under 2°C and 4°C warming scenarios show notable variation across seasons, despite overall annual wind driven rain changes being small or not practically significant. Figure A shows how in winter months wind driven rain is projected to increase from southern and westerly directions, particularly under 4°C warming. Meanwhile, summer wind driven rain projections see the opposite trend, with marked decreases in wind driven rain, particularly under 4°C warming. This means that wind driven rain exposure is projected to become more concentrated in winter months.

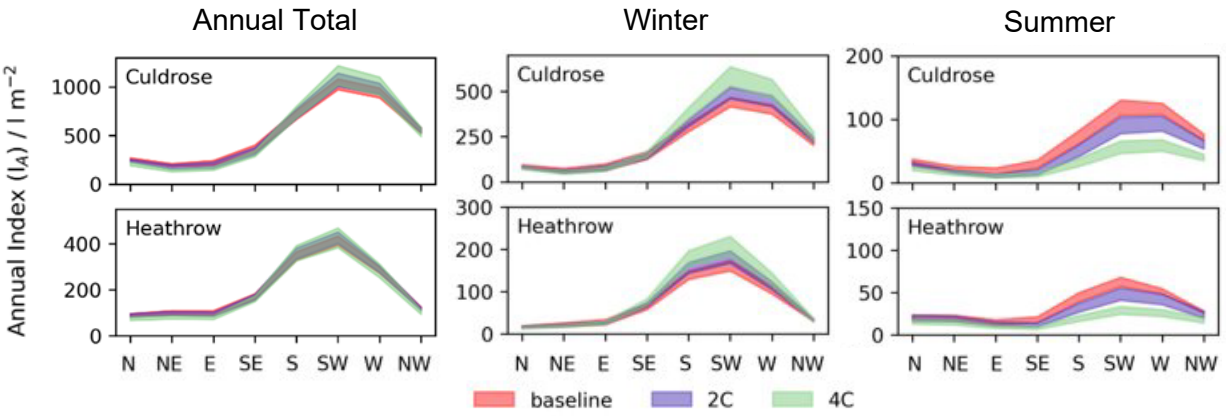

Figure A. Overview of changes in projected wind driven rain across seasons at specific weather station locations.

2. Under both 2°C and 4°C warming the changes in annual wind driven rain vary by orientation. As shown in Figure B when averaged across all orientations, there are negligible changes for 2°C warming, and only minor increases for 4C. However, this average masks more practically significant changes for specific orientations. Under both 2°C and 4°C there are projected to be marked increases in annual wind driven rain from the west, south west, and south; under 4°C warming this could be up to 25% more wind driven rain in some regions. Conversely there are notable decreases projected in annual wind driven rain from the north, north east and east, particularly under 4°C warming much of the country would see decreases of 15 to 25%.

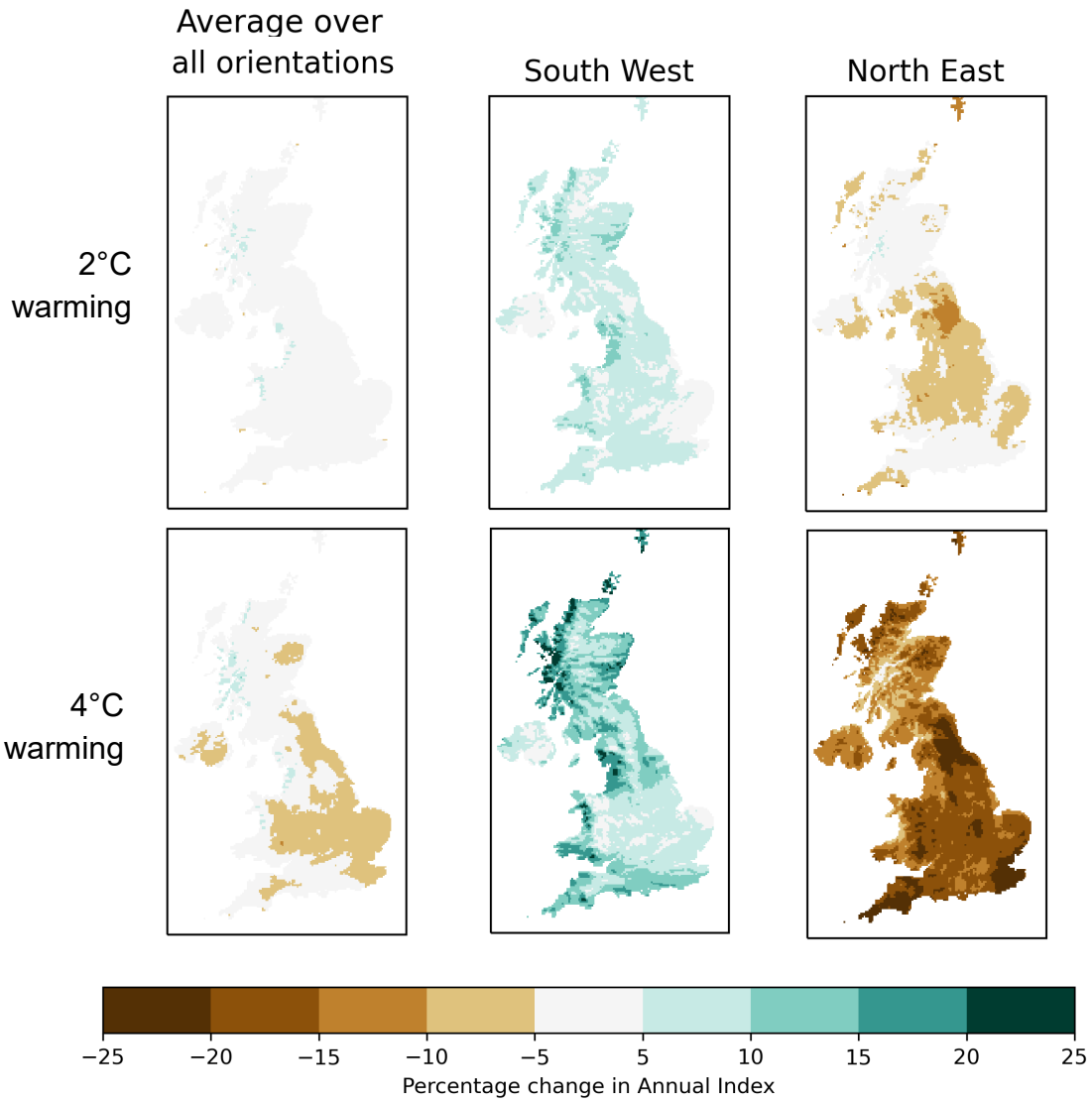

Figure B. Mapped overview of changes in annual wind driven rain for key orientations.

3. Analysing the quantity of wind driven rain in the 1 in 3 year spell (the worst case scenario you may expect every three years), which is used in Approved Document C to determine wind driven rain zones, shows this is set to decrease considerably under both 2°C and 4°C warming, despite the projected seasonal and directional changes in wind driven rain. Representative of a more extreme event, there is notable uncertainty around 1 in 3 year spell projections. It is also noteworthy that this decrease in magnitude of 1 in 3 year spell also coincides with a projected decrease in length of wind driven rain spells.

4. The duration of wind driven rain spells is an important factor, alongside quantity of wind driven rain, in determining impact on building fabric. This study used high spatial resolution hourly data from the UKCP18 climate projections which enabled analysis of changes in length of wind driven rain spells. The findings shown in Figure C illustrate how the number of medium (10 to 100h) and long (more than 100h) duration spells are predicted to decrease across the country, while short (less than 10h) spells will either remain as prevalent or increase for some locations. This means wind driven rain will be concentrated in fewer and shorter spells.

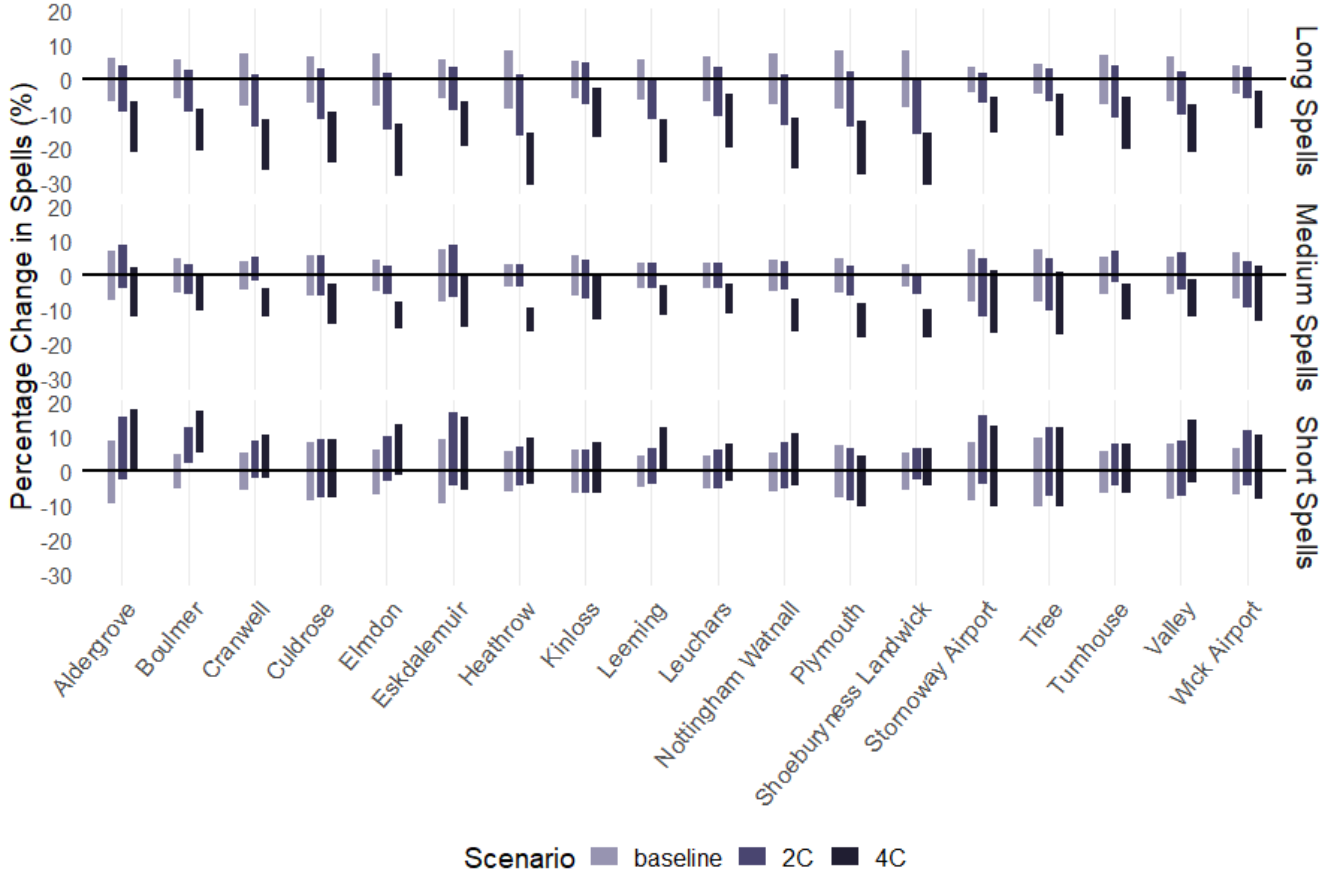

Figure C. Overview of changes in number of wind driven rain spells of short, medium, and long duration for specific weather stations under 2°C and 4°C warming.

While this study suggests that averaged across a year wind driven rain is not projected to change considerably under 2°C and 4°C, there will be more notable changes in seasonality, across directions, and in the spells and intensity of wind driven rain across the year. The regions set to be most affected by increases in wind driven rain from southerly and westerly directions are already mostly classed in Approved Document C as having ‘severe’ or ‘very severe’ exposure to wind driven rain, with guidance for insulation reflecting this. Further research and analysis is needed to determine the impact of these changes, including whether there may be opportunities for insulating more homes with cavity walls in future.

Technical Abstract

A new gridded wind-driven rain dataset has been created for the UK using hourly climate data from a set of high-resolution climate projections which form part of the UKCP18 climate projections. The airfield metric was calculated, which quantifies wind-driven rain in the absence of any obstructions. Other factors can be applied to the airfield metric to estimate the actual amount of rain deposited on a wall. Previous wind-driven rain datasets were created from weather station data, and so only consider a historical period. The new dataset includes a baseline period (1981-2000) and two future time periods corresponding to 2°C and 4°C of warming above pre-industrial levels. The potential impacts of climate change on wind-driven rain can also be included in any assessments of moisture ingress in buildings.

There is significant variation in the quantity and duration of wind-driven rain with wall orientation across the UK, in line with the prevailing wind directions (generally from west to south). Modelled and observed hourly precipitation totals and hourly wind speeds were compared to establish the level of agreement and whether bias-correction of the data was required. Wind-driven rain was quantified using an industry-standard metric (corresponding to the airfield metric). The wind-driven rain metric, lengths of wet spells and annual totals have been evaluated by comparison with the same indices calculated using hourly observations from weather stations. This was important to establish that the high-resolution climate simulations are fit for purpose.

At most weather stations, the modelled and observed indices have similar magnitudes and variation with wall orientation, suggesting the modelled values are well aligned with observations. The model also captured local effects, such as the maximum in wind-driven rain from easterly directions at Leuchars, which is located on a south-east facing coastline in central Scotland. It is important to note that the weather station data may not be fully representative of the grid-box averages simulated by the climate models in UKCP18.

Approved Document C[1] (ADC) includes a map of wind-driven rain zones (“Diagram 12”), which are based on the magnitudes of events with a return period of 3 years. Similar maps of wind-driven rain zones were created from the climate model data for each wall orientation and an average across all wall orientations. The 1 in 3 year wind-driven values derived from the climate model data are mostly larger than those shown in ADC but are closer in value to those calculated from weather station data in a study by Orr et al. (2018).

Analysis of wind-driven rain for warming levels of 2°C and 4°C above pre-industrial temperatures suggests that wind-driven rain could increase for southerly and westerly wall orientations at many sites across the UK during winter, increasing by as much as 25% in some regions, whereas a small decrease is found for north-facing walls. During summer, reductions in wind-driven rain are simulated across the UK for all wall orientations. Overall, there is no significant change in annual exposure to wind-driven rain when averaged across all directions.

[1] The Building Regulations 2010. Site preparation and resistance to contaminants and moisture. Approved Document C, HM Government.

The lengths of wind-driven rain spells are projected to decrease under a warmer climate, which might imply there would be more wind-driven rain in shorter spells. Further research and analysis is needed to determine the impact of these changes and what if any climate change adaptation guidance is necessary to address this.

Background

Rain penetration into a building refers to the ingress of rainwater above ground at various points in the external envelope, including the roofs, walls, chimneys and openings such as windows and doors. Here, the focus is on wind-driven rain, which occurs when rain falls obliquely due to a horizontal force on the raindrops caused by the wind (Gholamalipour et al., 2022). This moisture not only damages the fabric but also creates unhealthy conditions for occupants, together with less visible problems like poorer thermal performance. Wind-driven rain is distinct from other moisture-related problems, such as condensation, rising damp and spillage from gutters and downpipes.

Issues of dampness with cavity wall insulation are very rare but can occur where a building is exposed to high levels of wind-driven rain. Where rain penetrates the outer wall, most cavity wall insulation will absorb the moisture and retain it owing to the lack of ability to dry out. This can lead to thermal bridging in the cavity reducing performance of the fabric as well as more critically transferring moisture to internal walls, causing ongoing issues of damp and mould. This is why, in the UK, the suitability of cavity wall insulation is assessed following guidance and wind driven rain zones defined in Approved Document C (ADC; HM Government, 2004) of the Building Regulations, avoiding use of such insulation in locations with high exposure to wind driven rain.

In the UK, the risk of wind-driven rain is currently assessed using a dataset derived from about 30 weather stations around the UK. This dataset was used to produce a map of wind driven rain zones in ADC. The weather data used were recorded between 1959 and 1991 and were used in the creation of the British Standard BS:8104 for assessing exposure of walls to wind-driven rain. Owing to climate change and longer-term variability, this dataset is no longer fully representative of the current climate. For instance, global average surface wind speeds have fallen from the 1980s, a phenomenon known as global terrestrial stilling, although this trend has reversed from around 2010 (Zeng et al., 2019). Additionally, neither the British nor ISO standards provide information on possible future climatic conditions. This report describes the creation of an updated wind-driven rain dataset using high-resolution climate information from the United Kingdom Climate Projections 2018 (UKCP18; Lowe et al., 2018).

Introduction

Wind-driven rain refers to rain given a horizontal velocity by wind and falling obliquely (Gholamalipour et al., 2022). It is a significant environmental risk to many buildings; for example, it is a source of moisture that can drive swelling and shrinking of timber which can result in cracks and further deterioration (Richards and Brimblecombe, 2022). Wind-driven rain can penetrate walls leading to the growth of mould inside the building. It can also enhance failure of brick and stone via freeze-thaw cycles (Ruedrich et al., 2011) and encourage the growth of algae leading to discolouration and deterioration of the building surface (Gaylarde, 2020). Wind-driven rain is an important component of the risks to building fabric (Risk H5) identified in the UK Third Climate Change Risk Assessment (Kovats and Brisley, 2022) that requires further investigation.

Previous work

The first known study of wind-driven rain in the UK was by Lacy and Shellard (1962). They combined maps of annual average wind speeds and isohyets of annual rainfall totals to produce estimates of total wind-driven rain. They used the product of the rainfall totals in and wind speeds to calculate a driving rain metric (W) with units of $m^2\ s^{-1}\ year^{-1}$.

$$W = rv \tag{1}$$

where r is the rainfall total (expressed in metres per year) and v is the annual mean wind speed (in metres per second). This work was subsequently used to estimate relative annual exposures across the UK (Lacy, 1976). Prior (1985) updated this earlier work by calculating directional wind-driven rain exposures based on wind directions recorded at over 30 weather stations across the UK. Prior (1985) calculated a similar metric (W) which was the product of the rainfall amount (r), wind speed (v) and angle between the wind direction (d) and wall orientation (θ):

$$W = rv\cos(d - \theta) \tag{2}$$

These methods and results were used to create the British Standard BS:8104 on wind-driven rain (BSI, 1992). The exposure reference maps in this standard were based on meteorological data recorded between 1959 and 1991 (Orr and Viles, 2018). The “maximum wall spell index” from BS:8104 (an event with a return period of 3 years) was used to produce a map of wind driven rain zones in Approved Document C (ADC) of the building regulations.

Later, Orr and Viles (2018) used a metric from ISO 15927-3: 2009 (International Organization for Standardization, 2009) to assess wind-driven rain exposure on hourly timescales:

$$I = \frac{2}{9} v r^{8/9} \cos(d - \theta) \tag{3}$$

where I is the wind-driven rain metric (units: litres $m^{-2}\ hour^{-1}$). This metric is the airfield metric, which quantifies wind-driven rain in the absence of any obstructions. This equation appears to

be based on one derived by Lacy (1977) from earlier measurements of raindrop sizes and their terminal velocities. The metric is similar to the equation used by Prior (1985). Orr et al. (2018) used this metric to assess possible changes in the wind-driven rain risk at eight locations in the UK for 2070-2099. They used hourly data from weather stations and a weather generator that was part of the UKCP09 climate projections (Jones et al., 2009) to create future climate data. Their study showed that for the locations analysed wind driven rain was expected to increase in intensity with greater frequency of short spells leading to more consistent moisture exposure. They suggested such conditions would lead to greater moisture cycling, deep-seated wetting, and ultimately building element failure in vulnerable buildings.

This study

The aim of this study was to create a gridded dataset of wind-driven rain on hourly timescales for three time periods: a baseline (1981-2000) and time periods corresponding to global warming of 2°C and 4°C above pre-industrial levels, which are recommended for adaptation under current government policy (Watkiss and Betts, 2021). Wind-driven rain will be calculated using the airfield metric (Orr and Viles, 2018), which quantifies wind-driven rain in the absence of any obstructions such as trees and buildings. The United Kingdom Climate Projections 2018 (UKCP18; Lowe et al., 2018) include hourly climate information produced with a convection-permitting model (CPM) which has a resolution of 2.2 km (Kendon et al., 2023a,b). High time-resolution data are important for proper assessment of weather impacts on buildings (Brimblecombe and Richards, 2023). Wind driven rain was calculated for wall orientations corresponding to the cardinal and ordinal points of the compass as shown in Figure 1. To avoid confusion, “direction” will be used to refer to meteorological wind direction and “orientation” will be used for a hypothetical wall facing a given direction.

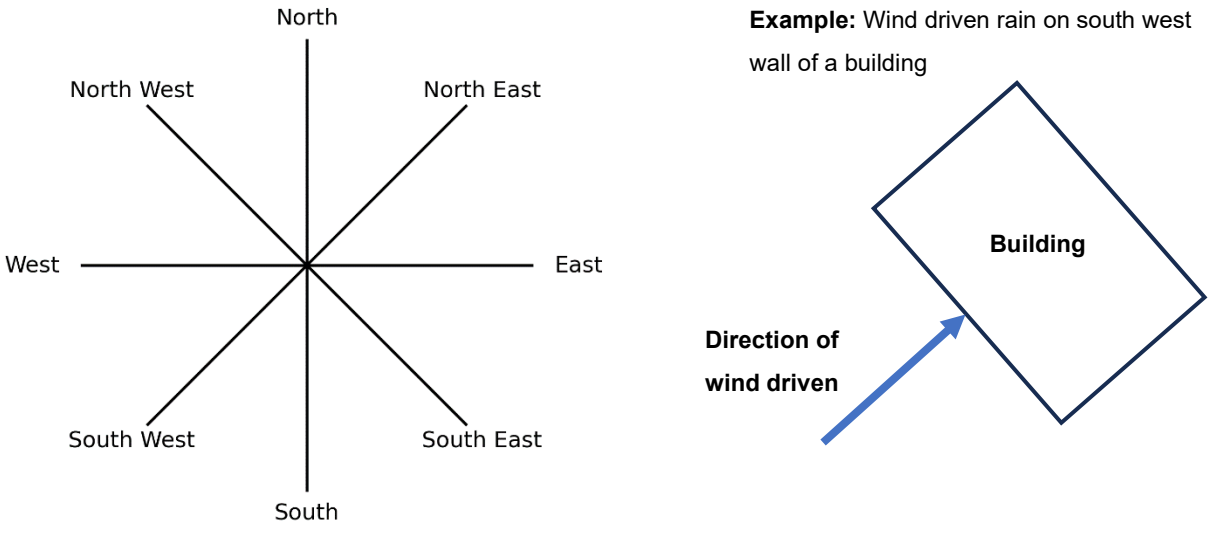

Figure 1. Eight wall orientations used to assess wind-driven rain. They correspond to the cardinal and ordinal points of the compass. Example given to illustrate for case of wind driven rain on south west wall of a building.

In the following sections, the datasets used are introduced and the modelled data are evaluated by comparison with weather station data. Next, the wind-driven rain metric is introduced alongside other statistics. Finally, projected changes in the wind-driven rain metric are shown and analysed.

Datasets

UKCP18 climate projections

The UKCP18 climate projections (Lowe et al., 2018) were created using simulations from three sets of models: global, regional and convection permitting (Figure 2). Initially, simulations were completed for 1899-2099 using fifteen versions of the Hadley Centre's global climate model HadGEM3-GC3.05, and 13 projections from models that informed the IPCC 5th assessment (CMIP5). Simulations for future periods used greenhouse gas concentrations from the RCP8.5 scenario. Climate data from twelve of the HadGEM3 simulations for 1980-2080 were used to drive a regional model whose domain included Europe and the northern Atlantic. The reasons why only 12 models were downscaled and the selection of those models are described in section 4.3 of the UKCP18 Land Projections report (Murphy et al., 2018).

Figure 2. Maps showing the resolution of the global (orange), regional (green) and convection-permitting ("CPM") climate models used to produce the UKCP18 climate projections. The inset boxes indicate the number of ensemble members. The global projections include 15 versions of the Hadley Centre's model HadGEM3-GC3.05 and results produced by 13 models from other climate centres. This image © Crown Copyright 2018.

These twelve regional model simulations were subsequently used to drive a convection-permitting model (CPM) which had a resolution of 2.2 km (Kendon et al., 2023a,b). Hourly climate data (rainfall totals and wind speeds) were archived from the CPM simulations. These data have been aggregated to a regular 5 km grid on the Ordnance Survey National Grid (Ordnance Survey, 2020) to enable comparisons with other UK-based datasets; the 5 km data will be analysed in this study. These hourly data are available for a 100 year period, from December 1980 to November 2080 (Kendon et al., 2023a,b).

Climate models simulate wind vectors along lines of constant latitude and longitude; these vectors can be used to calculate wind speeds and directions. The UKCP18 projections include hourly mean wind speeds calculated from these vectors on the 2.2 km grid, which have been aggregated to the 5 km grid. However, wind directions are not supplied. Only daily mean

values of the wind vectors were aggregated to the 5 km grid; hence, wind directions could only be calculated on daily timescales. A comparison was made of daily mean and hourly wind directions recorded by each weather station. In most cases, the daily mean direction reflected the dominant direction in the hourly data on the same day. For a few stations, larger differences were seen. For example, at Plymouth, when the daily mean direction was southeasterly, similar numbers of easterly and southeasterly winds were recorded in the hourly data. Some bias in the directions will therefore be present in the hourly wind-driven rain data.

HadUK-Grid

HadUK-Grid is a collection of gridded climate variables derived from the network of UK land surface observations (Hollis et al., 2019). The climate data have been interpolated from meteorological stations onto a uniform grid to provide complete and consistent coverage across the UK. The datasets cover the UK at a resolution of 1 km × 1 km but have been aggregated to the same 5 km grid as the CPM data. HadUK-Grid does not include the Republic of Ireland. The Irish Meteorological Service (Met Éireann) have produced gridded datasets of temperatures and rainfall for the Republic of Ireland but not wind speeds.

Weather stations

Hourly values of wind speeds, wind directions and rainfall totals were extracted from the Met Office's MIDAS database (Met Office, 2019) for eighteen weather stations shown in Figure 3 (the locations of these stations are listed in Table A1 in the Appendix). These stations were chosen as hourly data for 1981-2000 were available, enabling use in validation of modelled wind driven rain outputs from climate projections. Most of them are located at low altitudes on airfields or airports where interference from buildings, trees and other obstructions would be minimal. No stations were found for inland areas of Wales and Scotland, and only one station was identified in Northern Ireland. Only one station (Eskdalemuir) is located on an exposed hilltop site. Subsets (8 and 9) of these stations were used by Orr and Viles (2018) and Orr et al. (2018) respectively.

An examination of the weather station data showed that the rainfall amounts were archived to one decimal place, so the smallest value recorded is 0.1 mm per hour. Wind directions are rounded to the nearest 10° and were in the range 10° – 360°. All instances of 360° were changed to 0° before analysis. Wind speeds are recorded in whole numbers of knots and so are only available in steps of about 0.51 m s^{-1}. The lowest wind speed archived is 1.03 m s^{-1} (corresponding to 2 knots).

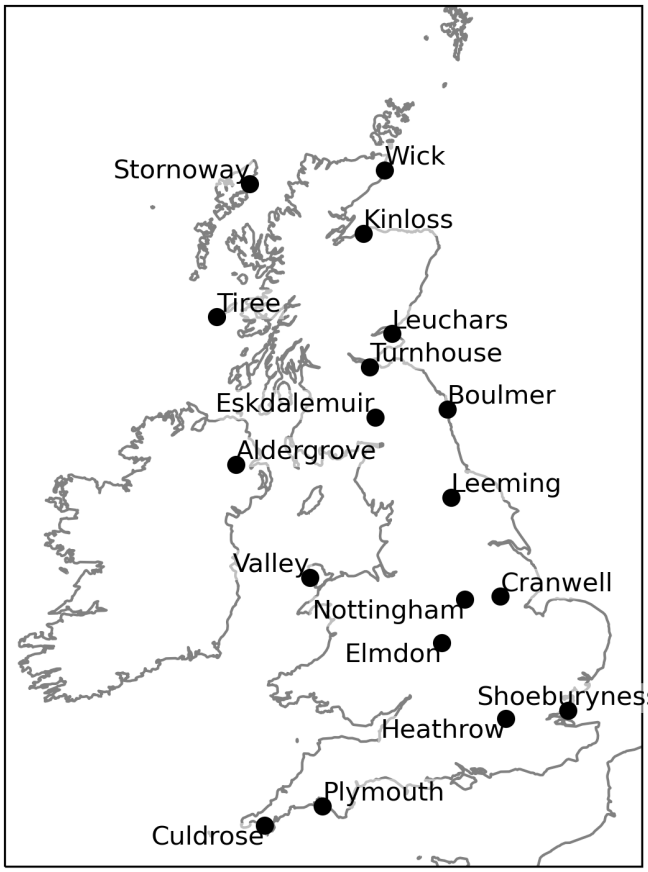

Figure 3. Locations of weather stations. Climate data from these stations were used to evaluate the CPM simulations. Their locations are listed in Table A1.

AgERA5

The AgERA5 dataset (Boogaard et al., 2020) provides gridded daily surface meteorological data for the period 1979 to present at spatial resolution of 0.1° (which is approximately 9 km over the UK). AgERA5 is based on the fifth generation of the European Centre for Medium-Range Weather Forecasts (ECMWF) atmospheric re-analyses of the global climate, better known as ERA5. AgERA5 was created for users in the agricultural domain. The correction to the 0.1° grid was achieved by applying grid and variable-specific regression equations to the ERA5 dataset interpolated at 0.1° grid. The equations were trained on ECMWF's operational high-resolution atmospheric model (HRES) at a 0.1° resolution. This way the data are tuned to the finer topography, finer land use pattern and finer land-sea delineation of the ECMWF HRES model. Meteorological variables in AgERA5 include temperature, precipitation, wind speeds and direction, humidity, cloud cover and radiation.

Global mean temperatures

Projections of wind-driven rain are required for two time periods corresponding to when global mean temperatures are 2°C and 4°C above pre-industrial levels. The global UKCP18 projections only begin in 1899, and the CPM data in December 1980. Six different datasets describing the change in global mean temperature (GMT) from the pre-industrial period (defined as 1850-1900) to the present day are available from the Met Office Climate Dashboard[2]. The period 1850-1900 does not represent the true pre-industrial climate, but it is the earliest time for which worldwide observations are considered extensive enough and reliable enough to provide a baseline for estimates of global mean temperatures (Hanlon et al., 2021). Twenty year periods corresponding to the years when the Earth's climate could become 2°C and 4°C warmer than the pre-industrial period are shown in Figure 4 and are listed in Table A2 in the Appendix.

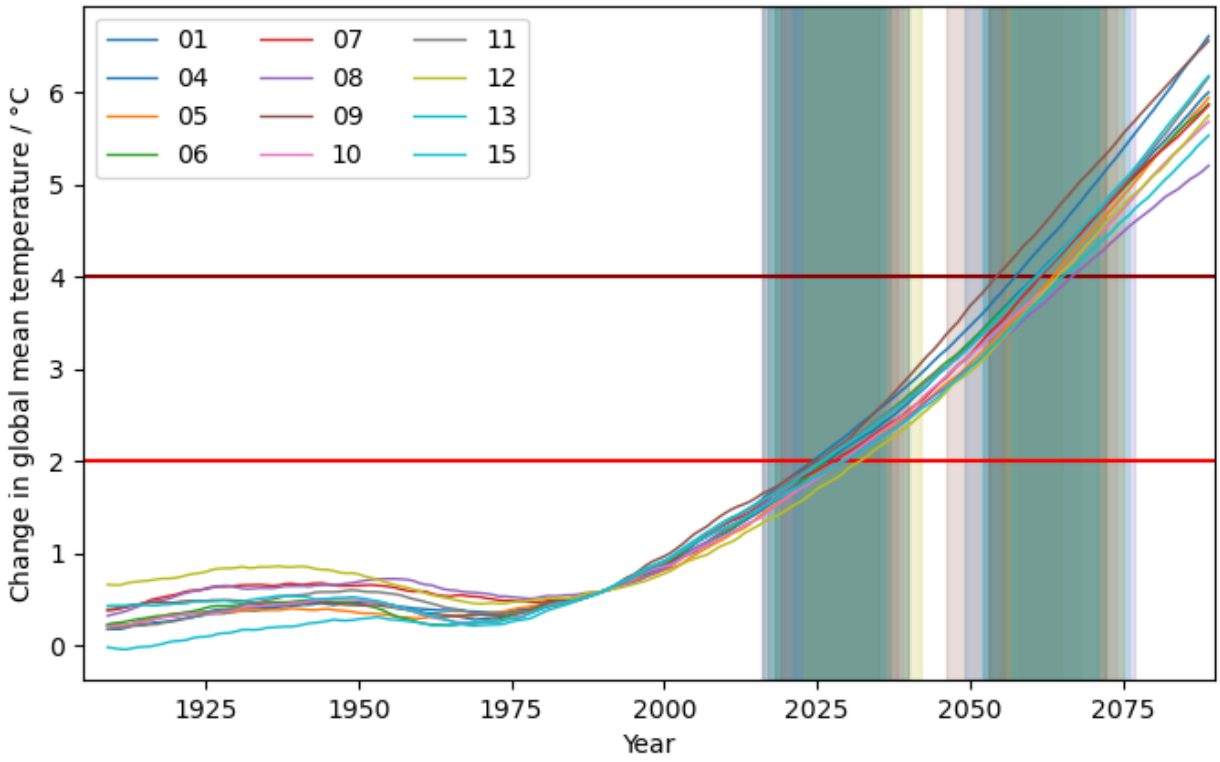

Figure 4. Estimated 20 year periods when global mean temperatures could reach 2°C and 4°C above pre-industrial temperatures. The red and brown horizontal lines represent global mean temperature changes of 2°C and 4°C relative to the pre-industrial period (defined as 1850-1900). The two shaded areas centred around 2040 and 2065 indicate when each UKCP18 ensemble member reaches 2°C and 4°C. The 12 coloured lines represent temperature changes from each of 12 UKCP18 global simulations that were downscaled. The 20 year periods when global mean temperatures could reach 2°C and 4°C are listed in Table A2.

[2] https://climate.metoffice.cloud/

These twenty year periods were calculated as follows. The change in GMT from the pre-industrial period to the UKCP18 baseline period (1981-2000) was calculated as the average change from the six datasets on the Climate Dashboard. Next, changes in GMT between the baseline period and all years to 2080 were calculated from the UKCP18 global climate simulations, focusing on the same 12 ensemble members that were downscaled. The change in temperature between the pre-industrial and baseline periods was added to the modelled temperature changes. Twenty year periods centred on the year when GMT exceeded 2°C and 4°C were then identified in each of the UKCP18 global model simulations, and are listed in the Appendix, Table A2. Data for the same 20 year periods were extracted from the corresponding CPM simulations and used to calculate the wind-driven rain metric, I. The change in global mean temperature from the UKCP18 global models and the 20 year periods corresponding to 2°C and 4°C of warming are shown in Figure 4.

Evaluation of climate model data

In this section, climate data from the UKCP18 CPM (wind speeds, wind directions and precipitation totals) are evaluated using data for 1981-2000. First, previously published evaluations of the CPM are summarised. Next, modelled values of these three variables are compared with observed values from weather stations. This evaluation is needed to determine if the UKCP18 CPM data are fit for purpose and whether any bias-correction of the meteorological data is required. Finally, a simple driving rain index (not the same as I or IA above) is calculated from modelled and observed data to provide a first evaluation of wind-driven rain in the CPM.

Previous evaluations of the CPM

Extreme precipitation totals on hourly timescales from the CPM have been compared with hourly totals from CEH-GEAR1hr by Kendon et al. (2023a). CEH-GEAR1hr is a 1 km gridded dataset of hourly rainfall totals for Great Britain for the period 1990-2016 that was derived from surface rain gauge data (Lewis et al., 2018). Annual maximum hourly precipitation values from the CPM over south-east England and north-west England agreed well with the values from CEH-GEAR1hr. Kendon et al. (2023a) also showed that the modelled and observed numbers of events per year exceeding 20mm/h across the UK were in good agreement.

Kendon et al. (2023b) compared seasonal precipitation totals and daily extremes of precipitation in the CPM and HadUK-Grid (Hollis et al., 2019). HadUK-Grid is a gridded dataset which includes rainfall totals on daily, monthly, seasonal and annual time scales at a resolution of 1 km over the UK. Kendon et al. (2023b) showed that the modelled and observed precipitation totals were in good agreement in both cases. Kendon et al. (2023b) noted a tendency of the CPM to overestimate the intensity of heavy events in summer, which is a consequence of convection not being fully resolved at 2.2 km resolution. These authors also noted that the CPM simulates a very small number of very high daily rainfall totals, above 300 mm, which are judged to be unphysical; i.e., not realistic. The highest observed hourly rainfall total in the UK (at the time of writing) is 92 mm, which was recorded on the 12th July 1901 at Maidenhead, Berkshire (Hand et al., 2004). It is assumed this event could have happened anywhere within the UK. In this study, any modelled hourly rainfall total above 92 mm was set to 92 mm.

Wind speeds in the CPM were not compared with observed speeds from weather stations. The CPM wind speeds are averages over an area of 5 km × 5 km, whereas weather station wind speeds are values at a point. This scale difference might erroneously suggest there is a large error in the modelled wind speeds. Wind speeds from the CPM do contain a small positive bias (Kendon et al., 2023b). The wind speeds were bias-corrected using a quantile mapping method based on the Weibull distribution (Li et al., 2019), as described later. Wind speeds from AgERA5 were used as the “observed” data. The Weibull parameters (called scale and

shape) were found using equations derived from the first and second moments (Blischke and Scheuer, 1986; Kelly et al., 2014). This method is summarised in section A1 in the Appendix.

Comparisons of modelled rainfall with observed values

Kendon et al. (2023a,b) showed that hourly extreme rainfall totals in the CPM and observations agreed well, but they did not evaluate smaller hourly rainfall totals. Hourly rainfall totals from the CPM and weather stations were compared using data for 1981-2000. The numbers of modelled and observed rainfall events in bins with fixed widths of 1 mm were calculated. The resulting distributions are shown in Figure 5, where only events up to 25 mm h^{-1} are shown. The numbers of rainfall events in each bin and the range of values in the CPM compare very well with the weather station data (Figure 5(a) and (b)), although the numbers of rainfall events are larger in the CPM at some stations, e.g., Elmdon and Shoeburyness. From the above evaluations, it was concluded that the hourly rainfall totals from the CPM are sufficiently close to the observed totals that no bias-correction was required.

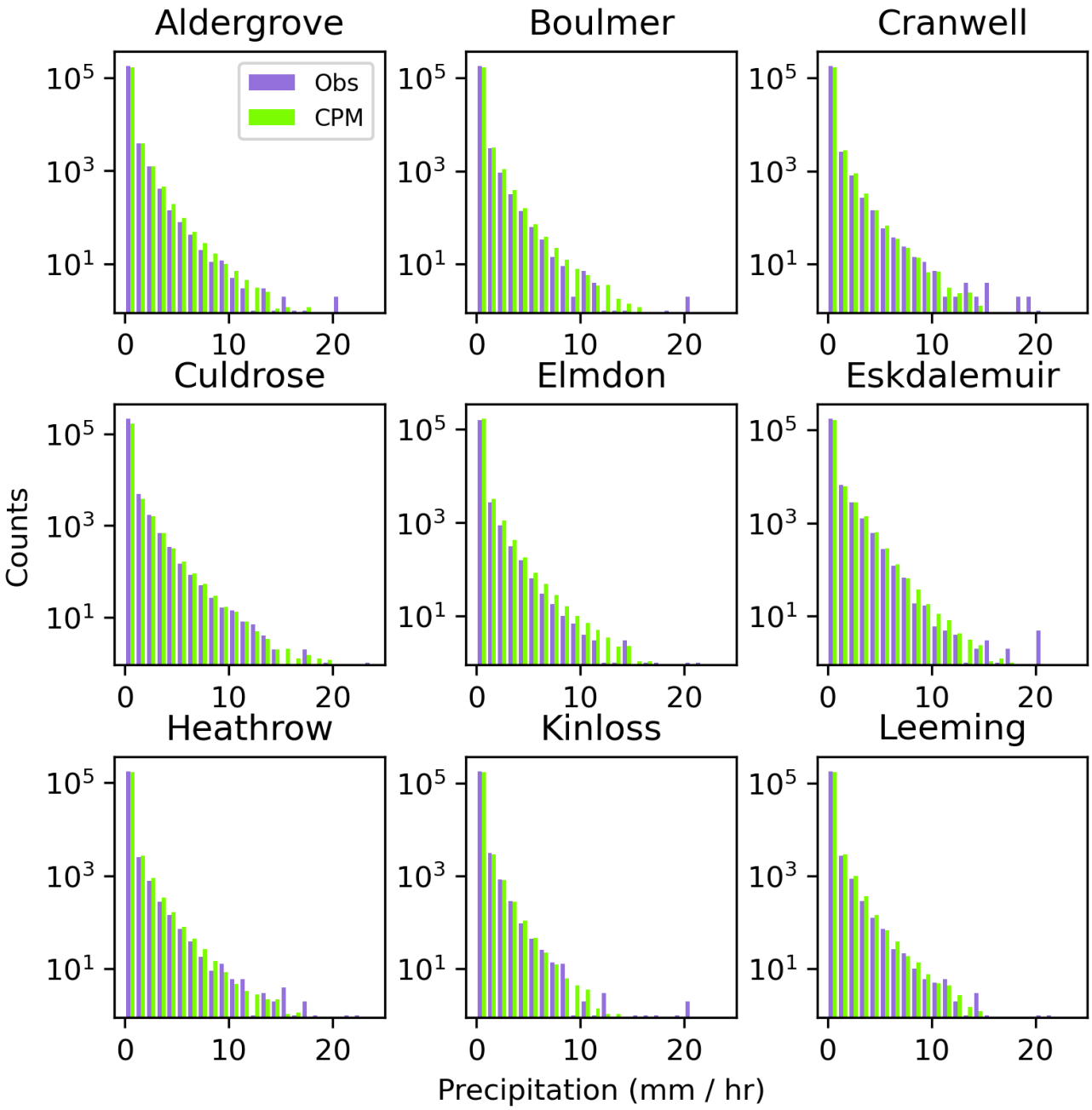

Figure 5(a). Histograms of counts of hourly rainfall totals within a year grouped in 1 mm bins. Counts are shown for weather station data (purple) and modelled data (green). The modelled data are ensemble means. Only bins up to 25 mm/h are shown.

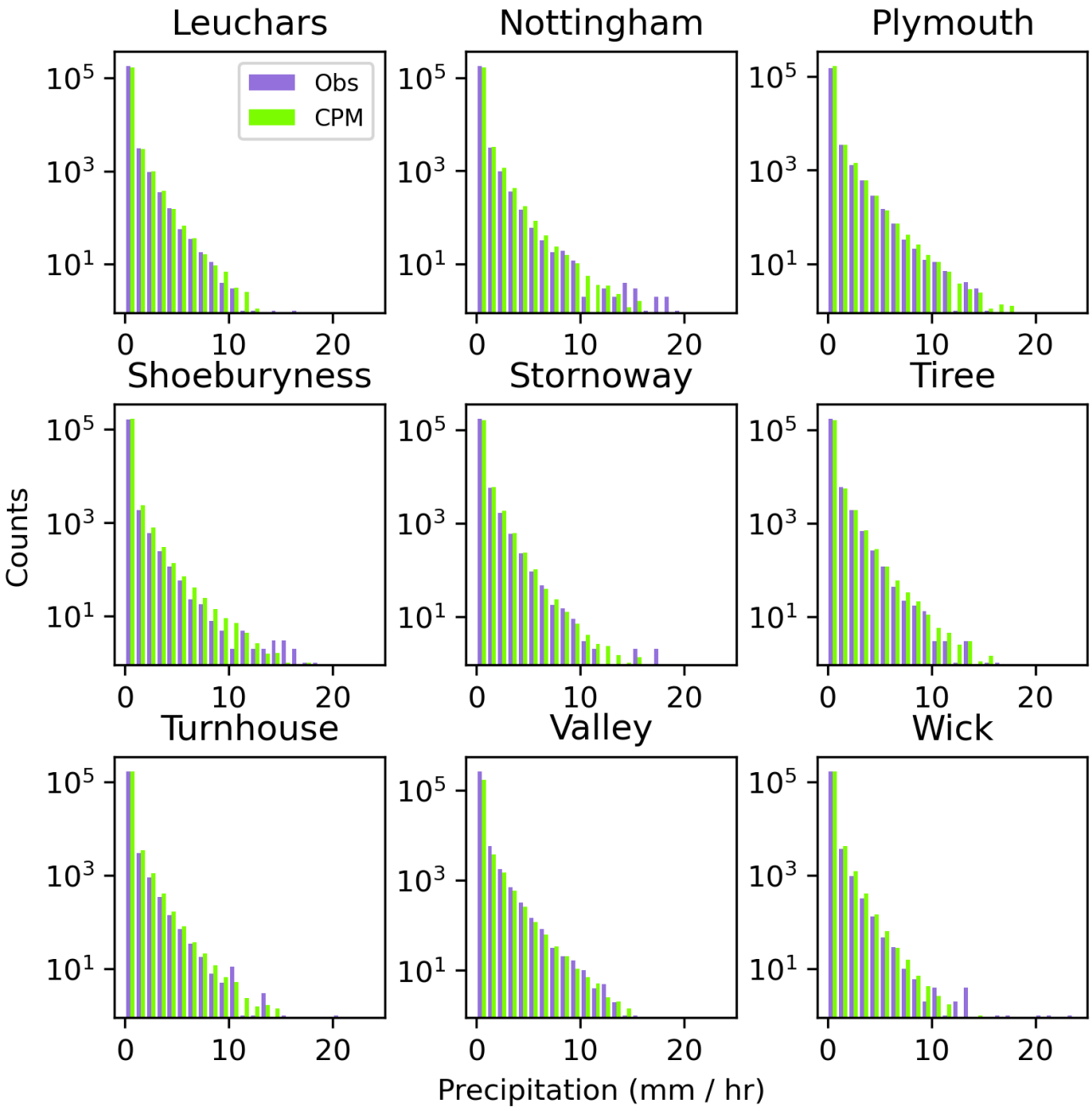

Figure 5(b). Histograms of counts of hourly rainfall totals within a year grouped in 1 mm bins. Counts are shown for weather station data (purple) and modelled data (green). The modelled data are ensemble means. Only bins up to 25 mm/h are shown.

Wind directions

The proportion of winds originating from each of the eight directions shown in

Figure 1 was counted using the observed directions from the weather stations and modelled directions from UKCP18 CPM ensemble member 1. For this comparison only, the winds directions in the CPM were rounded to the nearest 10° to match the observed data. The proportions of winds from each of the eight directions shown in

Figure 1 were then calculated following the procedure of Lea and Helvey (1971). Wind roses derived from the CPM and weather station data are shown in Figure 6. The CPM reproduces the proportions of winds from each direction for all stations reasonably well. It also reproduces the high proportions of easterly and westerly winds at Leuchars. However, the model underestimates the proportion of north-westerly winds at Leeming and the proportion of southerly winds at Stornoway. It also simulates higher percentages of westerly and south westerly winds at Eskdalemuir than are seen in the observations. Overall, the proportions of winds from the eight directions are in good agreement with the weather station observations, giving confidence in the modelled data. This result also shows that any bias in modelled wind directions introduced from the use of daily mean directions from the CPM is small.

UKCP18 CPM ensemble member 1	Observations from weather stations

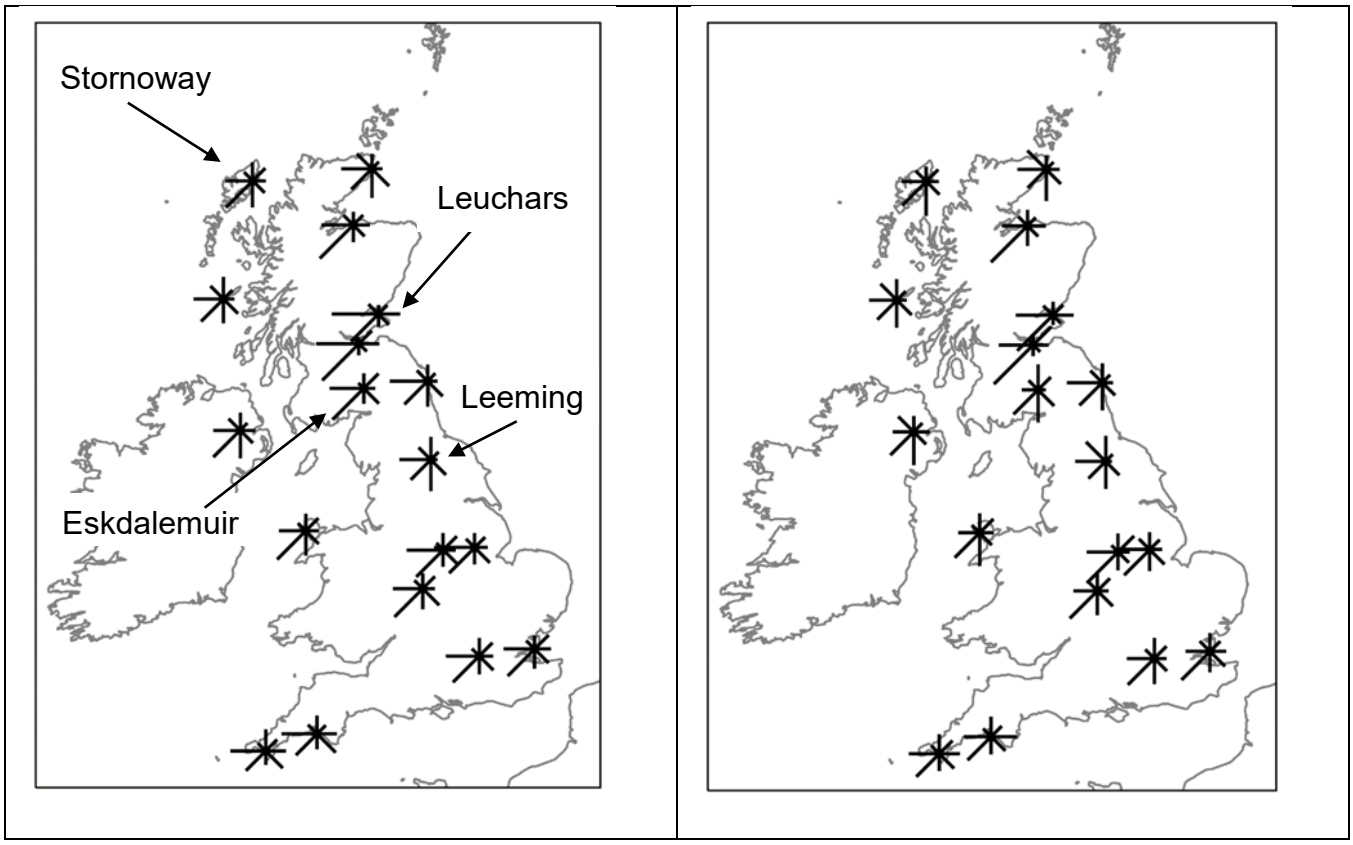

Figure 6. Wind roses for eight wind directions for 18 stations. The length of each vector is proportional to the percentage of winds from that direction for each station.

Climate models simulate wind speeds along lines of constant longitude and latitude. Overall wind speed and direction can be calculated from these two vectors. Any biases in wind directions in the CPM could not be corrected. AgERA5 provides wind speeds but not directions. Wind vectors along lines of constant longitude and latitude on hourly and daily time scales are available from the ERA5 reanalysis and the higher resolution product ERA5-land. However, wind speeds from these datasets are known to contain biases over the UK (Bloomfield et al., 2019). Hence, only overall wind speeds in the CPM could be corrected.

Driving rain index

In this section, maps of the simple driving rain index used by Lacy and Shellard (1962) are compared with values calculated from HadUK-Grid and the CPM (Figure 7). Comparisons of this index provides a first evaluation of wind-driven rain simulated by the CPM. A more detailed evaluation of the wind-driven rain metric is provided in a later section.

Lacy and Shellard (1962) combined maps of average wind speeds (in m s^{-1}) and isohyets of annual rainfall totals (converted to m y^{-1}) to produce estimates of driving rain (with units m^2 s^{-1} y^{-1}). This driving rain index is omnidirectional, because it is based on the wind speed but not wind direction. It is shown here to provide an initial evaluation of the modelled driving rain. The maps of rainfall and wind speeds used by Lacy and Shellard (1962) had been derived from observations made during the first few decades of the twentieth century. Maps comparing the

ensemble mean driving rain index calculated from UKCP18 with the same index calculated from 20 year means of wind speeds and rainfall totals from HadUK-Grid are compared with the map produced by Lacy and Shellard (1962) in Figure 7.

Although there are some detailed differences, the UKCP18 model reproduces the patterns and magnitudes of the driving rain index from HadUK-Grid very well. The modelled index has values less than 3 $m^2 s^{-1} y^{-1}$ over most of central and eastern England. It also reproduces the maximum of 15-20 $m^2 s^{-1} y^{-1}$ over western Scotland. The driving rain index in both maps increases from east to west. Similar patterns are seen in the map of Lacy and Shellard (Figure 7(c)). The main difference is that the area with driving rain index values less than 3 $m^2 s^{-1} y^{-1}$ in the UKCP18 and HadUK-Grid maps is larger than that in the map of Lacy and Shellard (unshaded area of Figure 7(c)). This area of the UK includes the relatively highly populated area of the West Midlands. This difference could be down to the different time periods of data used by Lacy and Shellard (1962) and the way the driving rain values were interpolated to create their map.

(a) UKCP18 ensemble mean

(b) HadUK-Grid

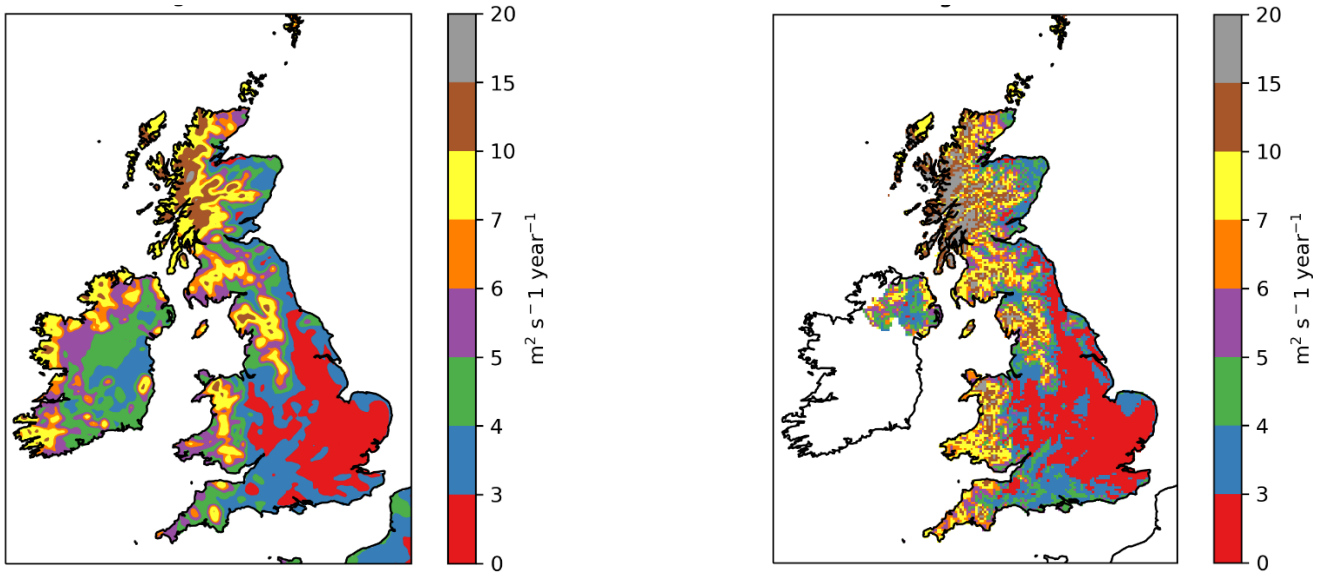

(c) Lacy and Shellard (1962)

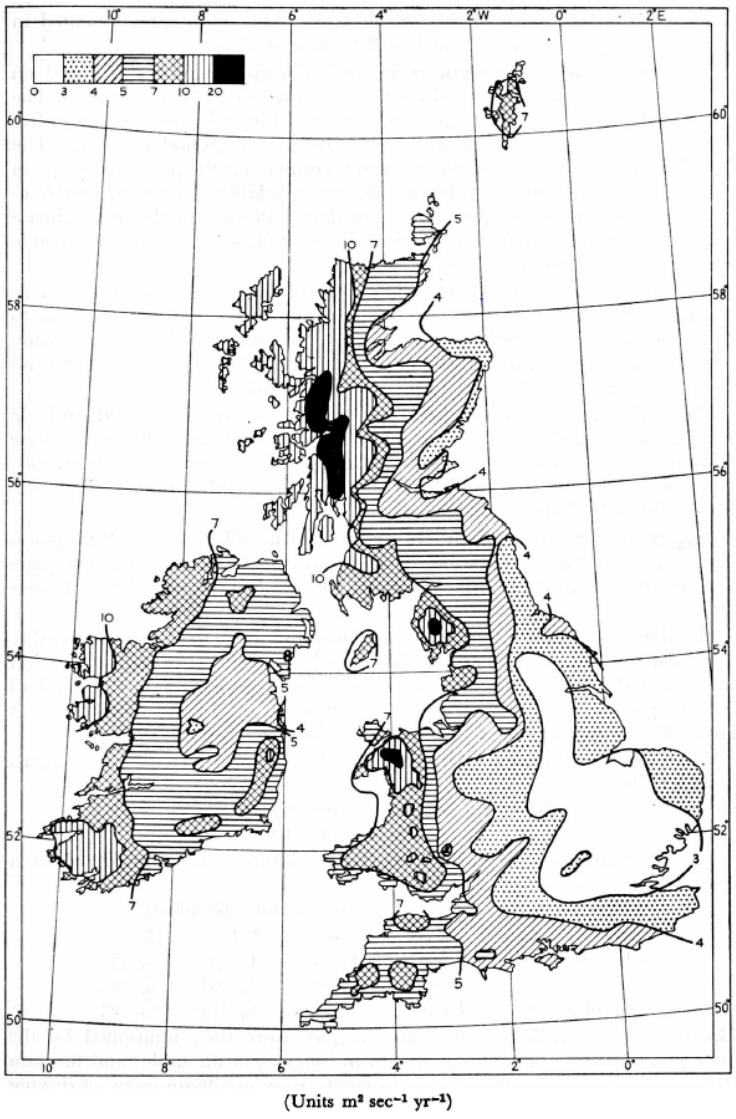

Figure 7. Maps of a driving rain index from (a) the mean of the UKCP18 CPM simulations, (b) HadUK-Grid and (c) Lacy and Shellard (1962). The driving rain index is the product of annual mean wind speeds and annual rainfall totals and has units of m^2 s^{-1} y^{-1}. The maps derived from UKCP18 and HadUK-Grid data were created using data for 1981-2000. HadUK-Grid does not contain data for the Republic of Ireland.

Wind-driven rain metric

The wind-driven rain exposure I in an hour is calculated using the equation from ISO 15927-3 (Orr and Viles, 2018), which is reproduced here:

$$I = \frac{2}{9} v r^{8/9} \cos(d - \theta) \quad (3)$$

where v is the hourly average wind speed (m s^{-1}), r is the hourly rainfall total (mm), and d and θ are the wind direction and wall orientation respectively, in degrees. I has units of l m^{-2} h^{-1} (litres per square metre per hour). I is only calculated when cos(d - θ) is greater than zero, i.e., when the wind would strike a given wall orientation. This metric is the airfield index, which quantifies the wind-driven rain in the absence of any obstructions.

The annual index I_A is the average of I over a number of years (Orr and Viles, 2018). Here, I_A was calculated separately for each year y, producing a series $I_A(y)$. I_A was then calculated as an average of $I_A(y)$ over all years:

$$I_A(y) = \sum I \quad \text{for all } I > 0 \ \text{ in year } y \quad (4)$$

$$I_A = \frac{1}{N} \sum I_A(y) \quad (5)$$

where N is the number of years.

A number of additional indices were calculated from the hourly time series of I. The spell specific index, $I_{s'}$, is the sum of I over each wet spell. A wet spell is defined as a period with wind-driven rain separated by more than 96 h with no exposure (Prior, 1985; Orr and Viles, 2018). BS:8104 did not consider the lengths of wet spells. Following Prior (1985), a threshold slightly larger than zero was used to distinguish times with or without wind-driven rain exposure. The threshold chosen was 0.001 l m^{-2} h^{-1}. The lengths of the wind-driven rain spells were also calculated.

Evaluating modelled wind-driven rain

In this section, the modelled annual index (I_A) calculated using the equations described earlier is evaluated. Maps showing values of I_A over the UK for each wall orientation are shown in **Figure 8**. These maps were created using data from all twelve UKCP18 CPM ensemble members. I_A was calculated as a 20-year average over the baseline period (1981-2000) from each member, then the average over all members was found. The largest values of I_A are seen for south, south-west and west-facing walls, where the greatest values are simulated over western Scotland. Considerably less wind-driven rain is simulated for walls with a northerly and easterly orientation. The areas with high and low values of the annual index averaged over all wall orientations (central panel of **Figure 8**) are broadly the same as the patterns in Figure 7.

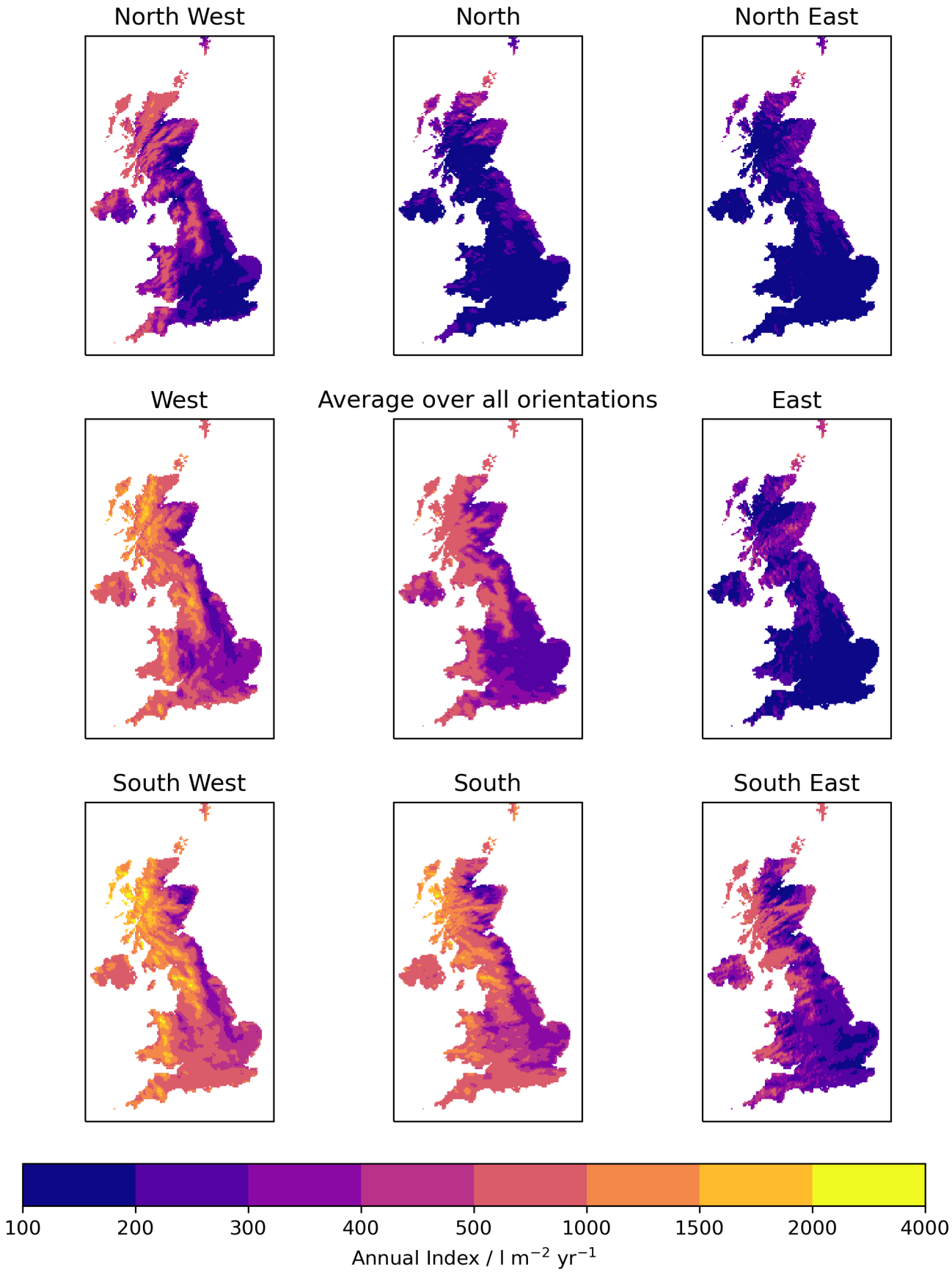

Figure 8. Maps showing values of the annual index (I_A) for each wall orientation averaged over the baseline (1981-2000) and all ensemble members. The map in the central panel shows the annual index averaged across all orientations.

In the remainder of this section, the wind-driven rain metric is evaluated over a range of time scales using data for 1981-2000. Hourly weather data from the weather stations were extracted from the Met Office's MIDAS database (Met Office, 2019). The UKCP18 model grid boxes in which the weather stations would be located were identified, so the wind-driven rain metric calculated using modelled and observed data could be compared at those locations.

Annual Index

The annual index (I_A) was calculated using hourly data for 1981-2000 from weather stations and compared with the modelled values shown in **Figure 8**. Values of I_A were calculated for each year, and then averaged over all years. The averaged values of I_A are shown as a function of wall orientation in Figure **9**.

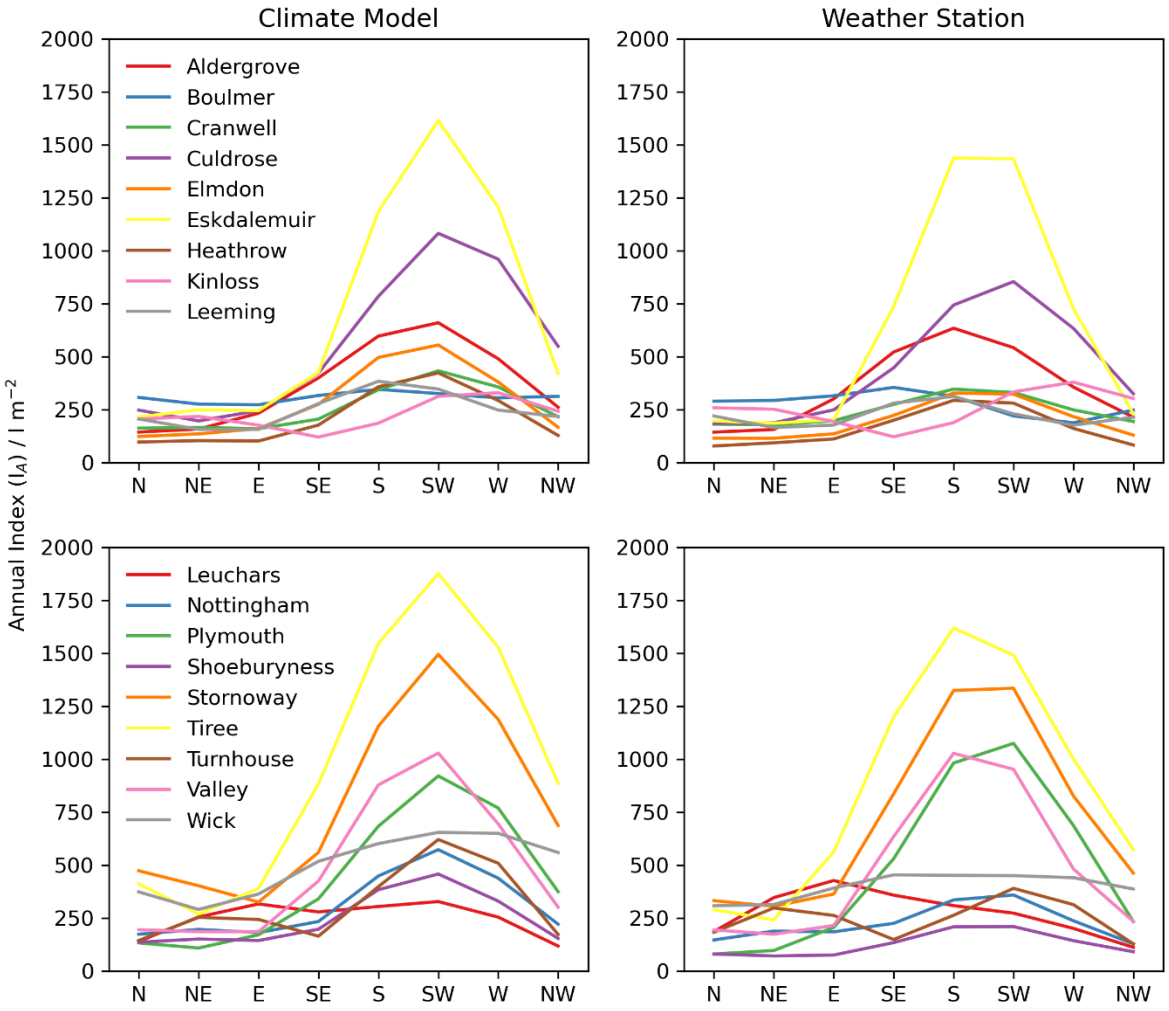

Figure 9. Annual Index (I_A) as a function of wall orientation, using data from the UKCP18 CPM, ensemble member 1 (left columns) and weather stations (right column). The weather stations are divided (arbitrarily) into two groups, split between the top and bottom row to aid readability. The weather station locations are shown in Figure 3.

Overall, the magnitudes of I_A calculated from the modelled and weather station data are similar at all locations, although the model overestimates the values of I_A for south and west-orientated walls at some of the southern stations. For weather stations exposed to westerly winds (Eskdalemuir, Tiree, Stornoway, Plymouth and Valley), the annual indices have a maximum for southerly and south-westerly directions. Kinloss is located on a north facing coast in Scotland and has two maxima for northerly and westerly directions. The CPM reproduces these two maxima. Leuchars is located on the eastern side of Scotland on a south-east facing coast and has a maximum in I_A for east facing walls. The CPM reproduces this maximum, but also has a secondary maximum for south-west facing walls. Aldergrove has a clear maximum in I_A for south facing walls using weather station data whereas in the model the maximum is seen for south-west and west facing walls. The model overestimates I_A at Shoeburyness. Values of I_A averaged across all wall orientations are listed in Table 1.

Table 1. Annual indices (I_A) averaged across all wall directions, calculated from hourly values of I from weather stations and the CPM.

Station name	I_A (station)	I_A (CPM)	Station name	I_A (station)	I_A (CPM)
Aldergrove	359	399	Leuchars	276	271
Boulmer	278	346	Nottingham Watnall	225	297
Cranwell	244	259	Plymouth Mountbatten	486	474
Culdrose	453	527	Shoeburyness Landwick	127	279
Elmdon	198	294	Stornoway Airport	723	868
Eskdalemuir	644	723	Tiree	872	874
Heathrow	162	231	Turnhouse	248	346
Kinloss	254	271	Valley	489	484
Leeming	222	254	Wick Airport	399	482

Directional Annual Index

The proportion of wind-driven rain from each of the eight wind directions is shown in a rose plot in Figure 10 for both the CPM and weather stations over the baseline period (1981-2000). The majority of wind-driven rain occurs from westerly, south-westerly and southerly directions at

most of the stations. The main exception is Leuchars, where a large proportion of wind-driven rain occurs from the east. A comparison of the roses derived from the CPM and weather stations show that the CPM underestimates wind-driven rain from the north-west and overestimates proportions from the west. Overall, the roses calculated from CPM and observed data are in reasonable agreement.

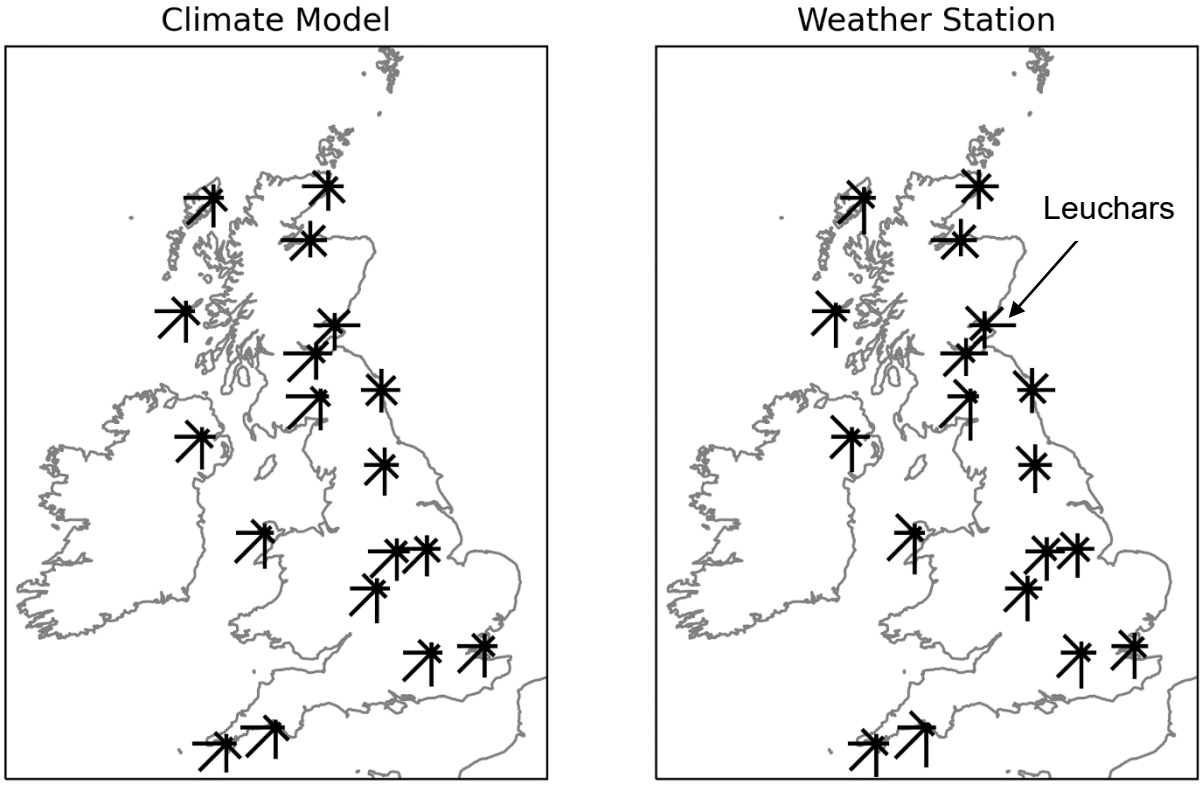

Figure 10. Annual relative driving rain index from eight wind directions. In each rose, the length of each vector is proportional to the percentage of the total index from that direction. Wind roses were derived from hourly CPM data (left panel) and hourly observations from weather stations (right panel).

A comparison of the roses in Figure 10 with those derived purely from wind direction (Figure 6) shows strong agreement between the prevailing wind directions in the UK and dominant directions in respect to annual relative driving rain index values. However, it also exhibits important differences. The proportion of winds from a southerly direction are notably lower than the proportions from the west and southwest (Figure 6). However, a large proportion of wind-driven rain occurs from southerly directions (Figure 10). At Leuchars, a large percentage of the winds come from easterly and westerly directions, whereas only a small proportion of wind-driven rain comes from the west, and the largest proportion is seen from the east. Overall, the modelled roses are generally in good agreement with those derived from weather station data. This result adds further confidence that the modelled data are fit for purpose, and wind-driven rain values from the eight directions calculated from the CPM are realistic.

Spell lengths

The frequencies of wet spell lengths as a function of wall orientation are shown in Figure 11, using data from weather stations and the CPM. The distributions of spell lengths in the model are in good agreement with those calculated from the weather stations. Short duration spells (up to 100 hours) have a maximum for north and north-east facing walls and a minimum for south and southwest facing walls. There is little variation in the number of spells with wall orientation for spells with lengths between 100 and 200 hours. Longer spells have a minimum between north and east and a broad maximum for southeast to west-facing walls. In the modelled data, the maxima for spell lengths longer than 500 hours occupies a smaller range of orientations (south to west) than is seen in the weather station data (southeast to west).

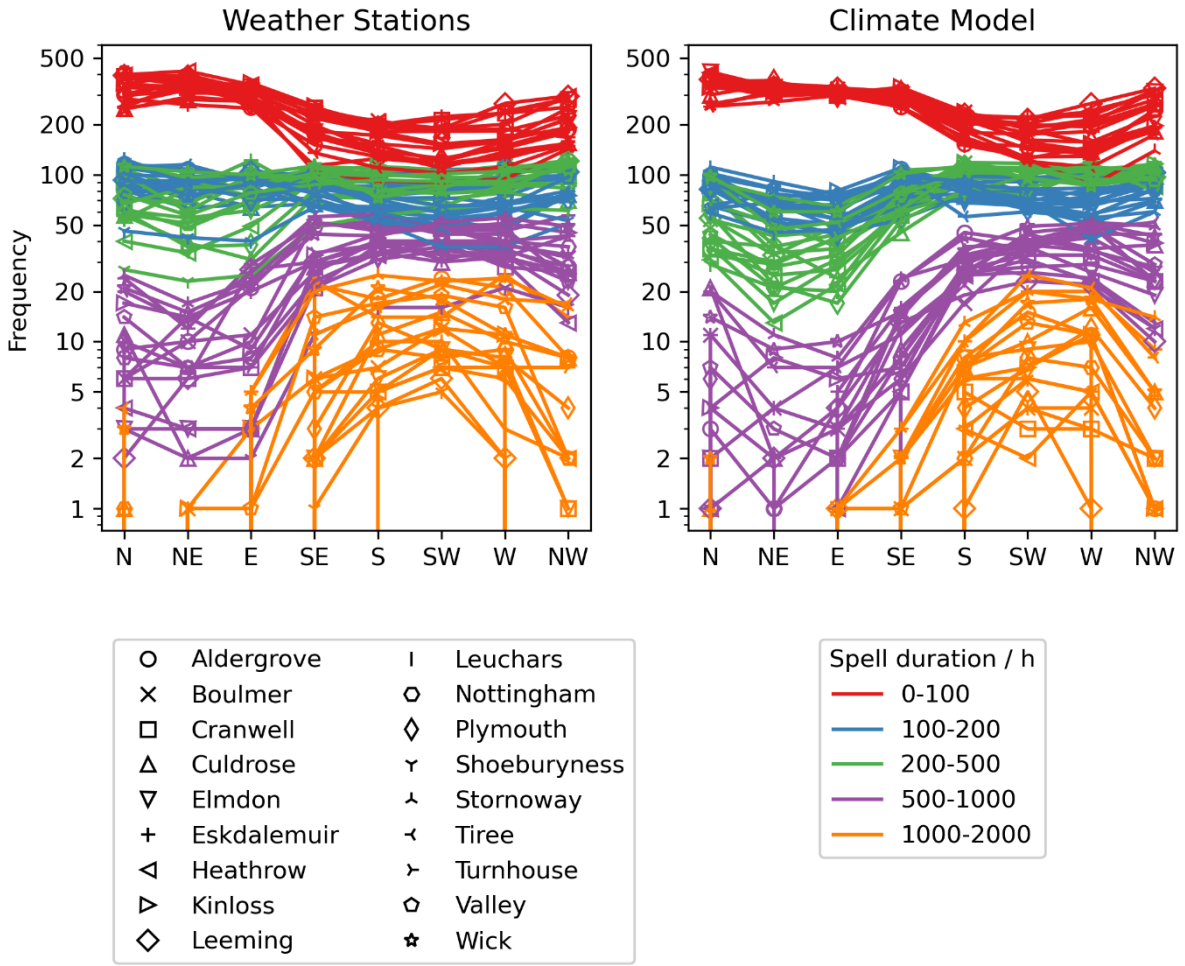

Figure 11. Frequency of wet spell durations (in hours) as a function of wall orientation for various weather stations. The colours show different ranges of spell lengths. The symbols represent data from each weather station.

Numbers of wet spells

The mean numbers of wet spells at each weather station are shown in Figure 12 as a function of annual total precipitation (panels a and c) and wall orientation (panels b and d). The numbers of spells are primarily controlled by the wall orientation, with more spells seen at all weather stations for walls facing north and east (panels b and d). There is also a weak dependence on the annual precipitation totals. Generally, there are slightly more wet spells for stations with lower annual precipitation totals (panels a and c), although the differences are small. This relationship is weaker in the CPM (panel c).

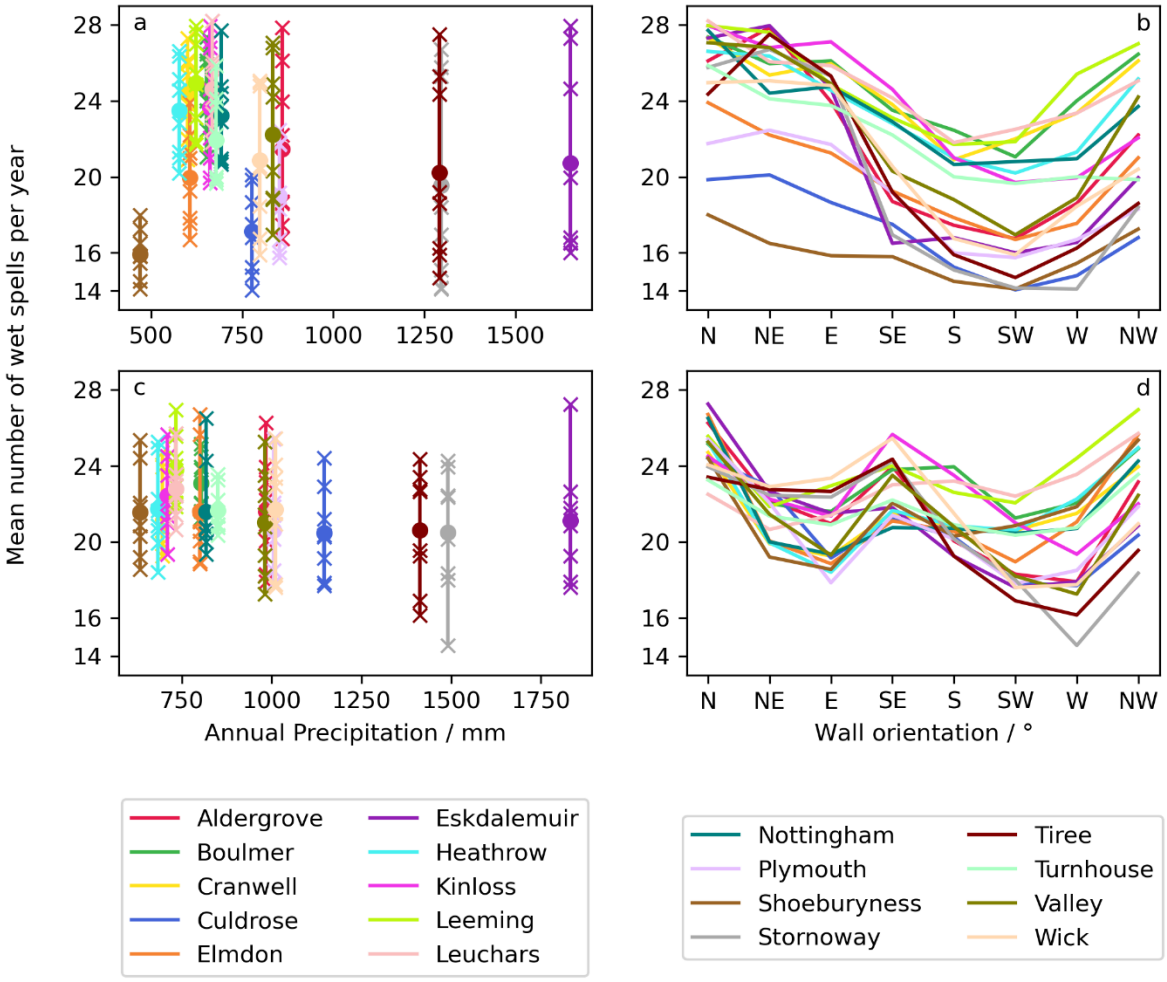

Figure 12. The number of wind-driven rain spells occurring at different weather stations as a function of average annual precipitation (left column) and wall orientation (right column). The upper two panels (a and b) show results using data from weather stations, and the lower two panels (c and d) show the same metrics calculated using CPM data. In panels a and c, the average number of spells per year across all wall orientations is represented by solid circles. The symbols ‘x' represent the annual average number of spells for different wall orientations at each site.

There are notably fewer numbers of wet spells for east-facing walls in the CPM than are seen in the weather station data (Figure 12, panels b and d). Pope et al. (2022) quantified large-scale circulation patterns over the UK in the UKCP18 global climate models. They used a set of 30 patterns which are currently used in operational medium- to long-range weather forecasting by the Met Office. These patterns were evaluated by Pope et al. (2022) by comparison with patterns generated from the ERA5 reanalysis (Hersbach et al., 2020). Five weather patterns are associated with winds with an easterly component over the UK. Pope et al. (2022) showed that the numbers of three of these patterns were underestimated by the UKCP18 global models during winter. This result might partially explain the drop in numbers of wet spells seen in the CPM data (Figure 12, panel d).

Active fractions

It is also useful to consider the 'active' fraction, which is defined as the fraction of hours within a wet spell during which rain was actually falling for a given location and wall orientation. The active fractions of wet spells in the weather stations and CPM are shown in Table 2 for three different spell lengths (as used by Orr et al., 2018). The 95% confidence intervals in the CPM data are lower as they are estimated using the entire ensemble. The average active fractions for short spells (less than 10 hours in length) across all of the stations are 0.91 and 0.90 from weather stations and the CPM respectively. For medium and long spells, the active fractions calculated from weather station data are about 0.24 and 0.13, whereas the averages from the CPM are 0.32 and 0.15. Longer spells have lower active fractions than shorter spells because they are more likely to include rainfall from several weather systems and include periods with no WDR. The active fractions in the model are larger than those in the weather stations for medium and long spells, suggesting modelled spells of rainfall might last longer but contain smaller rainfall totals for each hour.

Table 2. Active fractions of wind-driven, defined as the fraction of hours within a spell when rain was falling. The fractions shown are average values across all wall orientations for 1981-2000. Active fractions are listed from both weather station data ("Sta") and the CPM for each location. The errors are the 95% confidence intervals.

Station	Data Source	Short (Less than 10 h)	Medium (at least 10 h but less than 100 h)	Long (over 100 h)
Aldergrove	Sta	0.917 ± 0.013	0.232 ± 0.012	0.128 ± 0.003
	CPM	0.889 ± 0.004	0.323 ± 0.004	0.153 ± 0.001
Boulmer	Sta	0.904 ± 0.012	0.237 ± 0.012	0.114 ± 0.003
	CPM	0.900 ± 0.004	0.302 ± 0.004	0.133 ± 0.001

Cranwell	Sta	0.922 ± 0.011	0.226 ± 0.012	0.109 ± 0.002
	CPM	0.908 ± 0.003	0.300 ± 0.004	0.129 ± 0.001
Culdrose	Sta	0.908 ± 0.014	0.267 ± 0.015	0.143 ± 0.004
	CPM	0.913 ± 0.004	0.315 ± 0.004	0.163 ± 0.001
Elmdon	Sta	0.931 ± 0.011	0.243 ± 0.013	0.122 ± 0.003
	CPM	0.906 ± 0.004	0.315 ± 0.004	0.140 ± 0.001
Eskdalemuir	Sta	0.913 ± 0.014	0.247 ± 0.014	0.161 ± 0.004
	CPM	0.902 ± 0.004	0.402 ± 0.004	0.218 ± 0.001
Heathrow	Sta	0.917 ± 0.011	0.232 ± 0.012	0.112 ± 0.003
	CPM	0.911 ± 0.003	0.297 ± 0.004	0.130 ± 0.001
Kinloss	Sta	0.922 ± 0.012	0.218 ± 0.011	0.115 ± 0.003
	CPM	0.889 ± 0.004	0.299 ± 0.003	0.129 ± 0.001
Leeming	Sta	0.912 ± 0.012	0.234 ± 0.012	0.111 ± 0.003
	CPM	0.899 ± 0.004	0.304 ± 0.004	0.137 ± 0.001
Leuchars	Sta	0.917 ± 0.011	0.234 ± 0.011	0.112 ± 0.003
	CPM	0.901 ± 0.004	0.321 ± 0.004	0.136 ± 0.001
Nottingham Watnall	Sta	0.912 ± 0.012	0.233 ± 0.012	0.119 ± 0.003
	CPM	0.908 ± 0.004	0.320 ± 0.004	0.143 ± 0.001
Plymouth Mountbatten	Sta	0.921 ± 0.012	0.234 ± 0.012	0.138 ± 0.004
	CPM	0.907 ± 0.004	0.309 ± 0.004	0.158 ± 0.001
Shoeburyness Landwick	Sta	0.921 ± 0.012	0.211 ± 0.013	0.099 ± 0.003
	CPM	0.905 ± 0.003	0.280 ± 0.004	0.122 ± 0.001
Stornoway Airport	Sta	0.885 ± 0.018	0.247 ± 0.013	0.165 ± 0.004

	CPM	0.880 ± 0.005	0.353 ± 0.004	0.198 ± 0.001
Tiree	Sta	0.883 ± 0.016	0.259 ± 0.013	0.167 ± 0.003
	CPM	0.889 ± 0.005	0.332 ± 0.004	0.182 ± 0.001
Turnhouse	Sta	0.922 ± 0.011	0.241 ± 0.013	0.126 ± 0.003
	CPM	0.905 ± 0.004	0.332 ± 0.004	0.150 ± 0.001
Valley	Sta	0.922 ± 0.012	0.217 ± 0.011	0.122 ± 0.003
	CPM	0.902 ± 0.004	0.300 ± 0.004	0.141 ± 0.001
Wick Airport	Sta	0.908 ± 0.014	0.231 ± 0.013	0.126 ± 0.003
	CPM	0.883 ± 0.005	0.317 ± 0.004	0.156 ± 0.001

UK zones for exposure to driving rain: 1 in 3 year spells

Approved Document C (ADC; HM Government, 2004) includes a figure ("Diagram 12") showing four different exposure zones to wind-driven rain. These values of each zone were calculated using the "maximum wall spell index" from BS:8104, which are the magnitudes of 1 in 3 year wind-driven rain events (Orr and Viles, 2018). It is unclear whether the values in Diagram 12 are averages or maxima over all wall orientations. The four zones in Diagram 12 show wind-driven rain in ranges 0-33, 33-56.5, 56.5-100 and over 100 litres per m^2 per spell.

Orr and Viles (2018) calculated the magnitudes of 1 in 3 year wind-driven rain spells for 12 different wall orientations using data recorded at nine weather stations. They used data recorded over two periods, 1959-1991 and 1986-2015. Their "once every three years" spells are much larger than those shown in ADC. Using data for 1986-2015, the largest values for three stations (Aldergrove, Plymouth and Stornoway) lie between 350 and 500 litres m^{-2} per spell for south and west-facing walls. The smallest values, for north and east facing walls, range from about 31 to 100 litres m^{-2} per spell. For the earlier period (1959-1991), the 1 in 3 year events have different values. Those for Stornoway are larger, exceeding 550 litres m^{-2} per spell, whereas at Plymouth the maximum value is smaller, about 350 litres m^{-2} per spell. The smallest values are in the range 50 – 100 litres m^{-2} per spell. This result illustrates that the amounts of wind-driven rain in these spells is sensitive to the period chosen.

The amounts of wind-driven rain in 1 in 3 year spells were calculated using the CPM data from all 12 ensemble members for the baseline period and are shown in Figure 13. The 1 in 3 year spells were calculated for each of the eight wall orientations shown in

Figure 1 following a similar method to Orr and Viles (2018); see page 31.

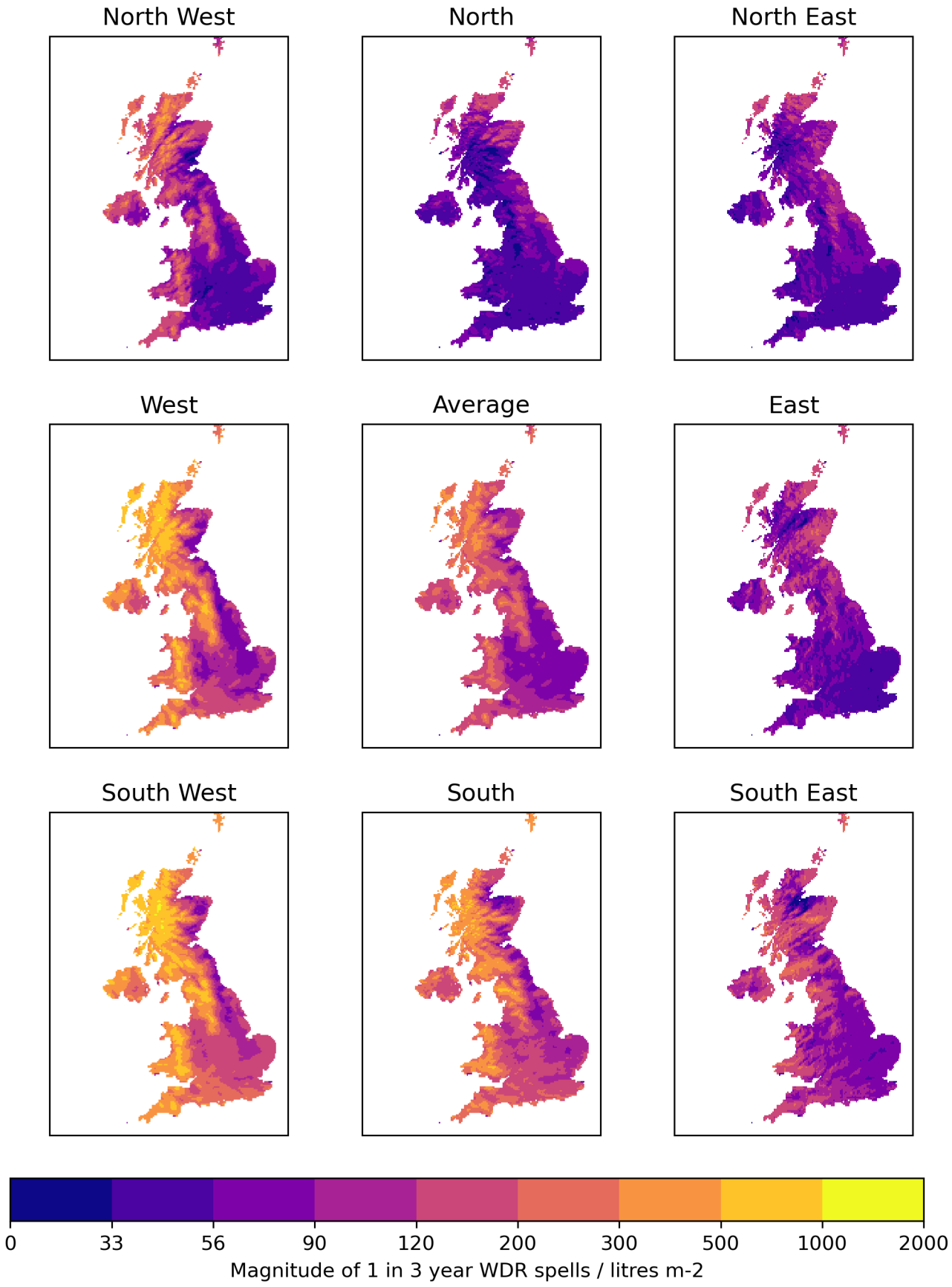

Figure 13. Exposure to wind-driven rain (in litres m^{-2}) for "one in three year spells" for eight wall orientations. The average across all wall orientations is shown in the central panel. Note that the scale is non-linear.

The magnitudes of wind-driven rain in 1 in 3 year spells were calculated as follows. First, the annual maximum wind-driven rain spell was found for each year and wall orientation. This procedure produces 20 values for each wall orientation. This number is relatively small for estimating 1 in 3 year events, so the annual maxima from all ensemble members were pooled together, to create a dataset with 12 × 20 = 240 values. A Gumbel distribution was fitted to the pooled annual maxima using maximum likelihood estimation. Examples of the fit of the Gumbel distribution to the pooled data are shown in the Appendix, Figure A1, using CPM data at the locations of the weather stations for south-west facing walls. For all locations, the Gumbel distribution is a good fit to the data. The Gumbel distribution was also a good fit to the pooled annual maxima for the other wall orientations (not shown).

The probability of occurrence (p) of a 1 in 3 year event is: $p = 1 – (1 / 3)$. The magnitudes of 1 in 3 year events were found by applying the probability p to the cumulative distribution function (CDF) of the fitted Gumbel distribution. The 1 in 3 year spells are shown in Figure 13 for all eight wall orientations. Average exposure across all orientations is shown in the central panel. These values are mostly larger than those in ADC but are similar to those calculated by Orr and Viles (2018).

Projected changes in wind-driven rain

In this section, projected changes in the wind-driven rain metric at each of the weather stations (Figure 3) are analysed. The times when global warming in each UKCP18 ensemble member reaches 2°C and 4°C above pre-industrial temperatures were calculated earlier; the twenty year periods for each ensemble member and time period are listed in the Appendix, Table A2. The wind-driven rain metric was calculated for each time period.

Projected changes in the annual index

The annual index was calculated for the baseline and periods corresponding to 2°C and 4°C of warming. Maps showing the percentage changes in the annual index using data averaged across the 20 year periods and ensemble members are shown in Figure **14** for 2°C and Figure 15 for 4°C of warming. Wind-driven rain from northerly and easterly directions is projected to decrease over most of the UK, whereas wind-driven rain from southerly and westerly directions is projected to increase. The largest increases are seen along west-facing coastal areas in the 2°C scenario, whereas more widespread increases are projected over large parts of the UK in the 4°C scenario. Under the 2°C scenario, the projected changes are between -20% and +15%. The projected changes are larger under the 4°C scenario, where they are as high as ±30%.

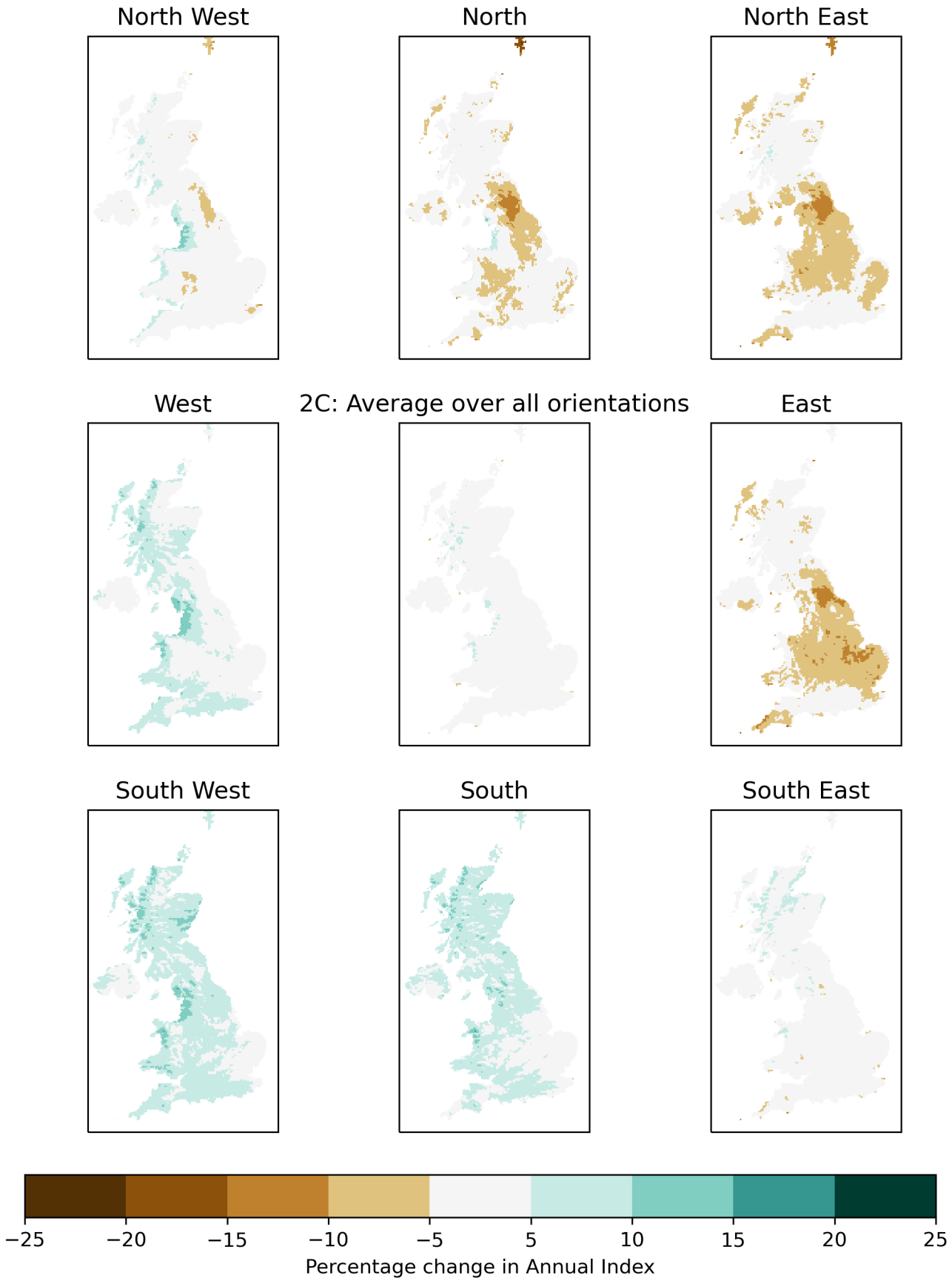

Figure 14. **Maps showing the percentage change in the annual index for 2°C of warming for each wall orientation. The changes shown are ensemble means averaged across 20 year periods corresponding to 2°C increase in GMT relative to pre-industrial temperatures.**

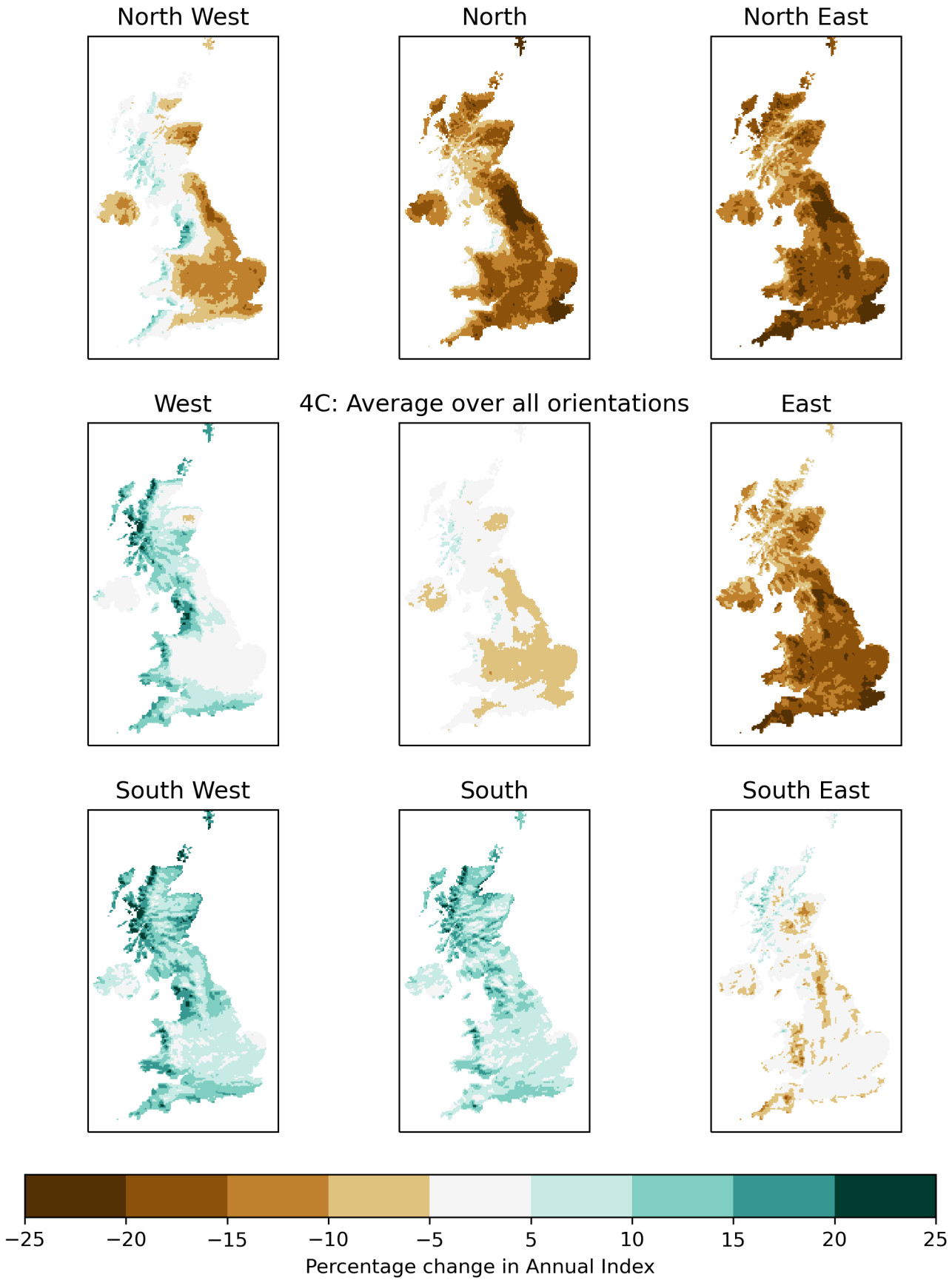

Figure 15. Maps showing the percentage change in the annual index for 4°C of warming for each wall orientation. The changes shown are ensemble means averaged across 20 year periods corresponding to 4°C increase in GMT relative to pre-industrial temperatures.

In the 2°C scenario, the largest relative decreases in wind-driven rain are projected over much of northern and central England, whereas under the 4°C scenario the greatest relative decreases are seen over north east England, the south west and south east corners. In contrast, the largest increases are seen over west-facing coastal areas, especially under the 4°C scenario.

The annual indices for all three time periods from the CPM at the locations of the weather stations are shown in Figure 16. The shaded areas represent the standard errors of the ensemble means. Little change in the annual indices is seen between the baseline and 2°C of warming. A small decrease is seen for north facing walls and a small increase is projected for south and west facing walls. Larger values of the annual index are projected at a number of stations under 4°C of warming, although the error in the mean overlaps with the errors in the baseline and 2°C periods. The largest projected increases in the annual index under 4°C of warming occur at sites with higher baseline values.

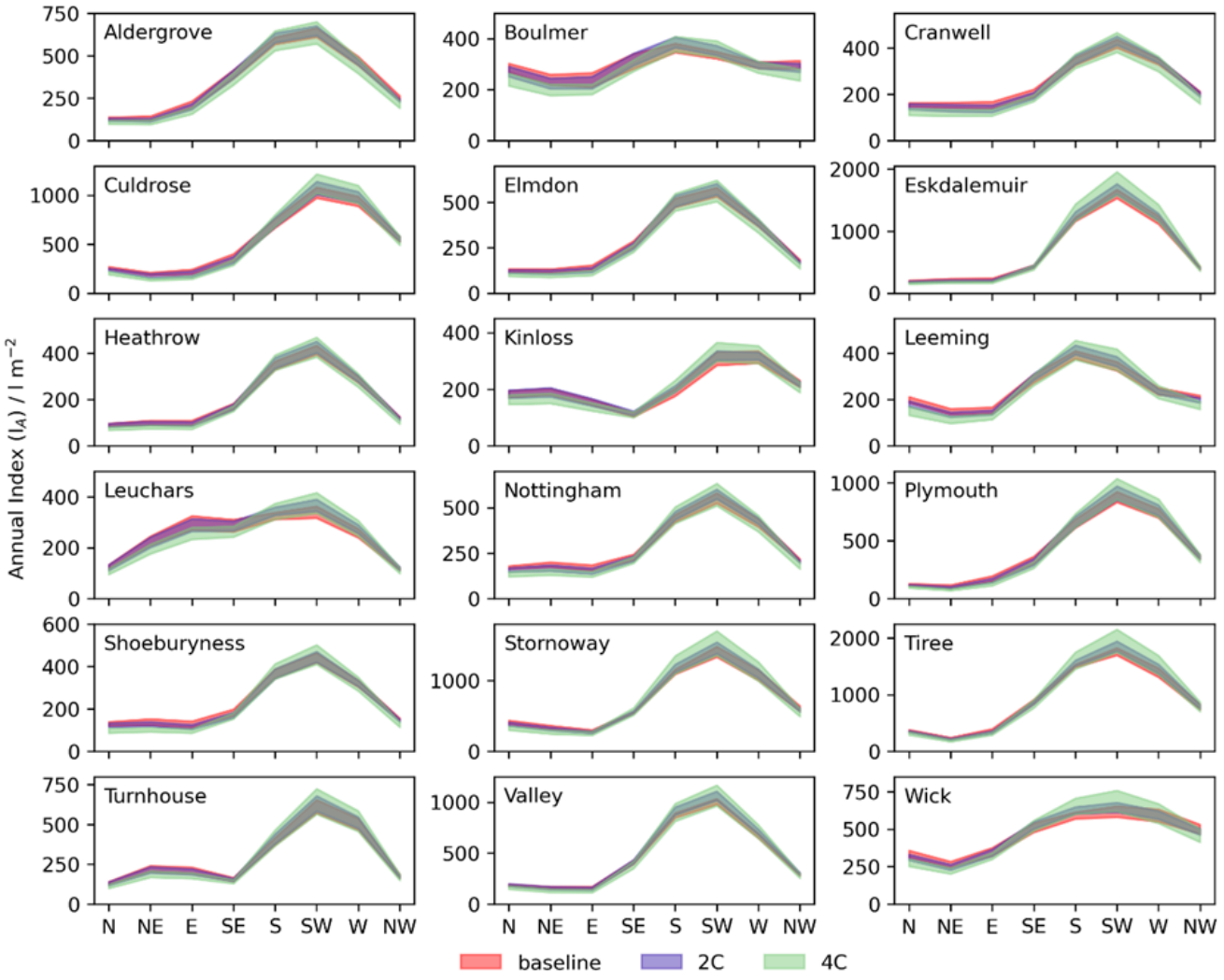

Figure 16. Annual index (I_A) as a function of wall orientation for the time periods corresponding to the baseline and times when global warming is 2°C and 4°C above pre-industrial levels. The shaded areas show the standard error in the ensemble means of the annual index.

While there was little difference found between annual indices for different levels of warming and the baseline, the seasonality of wind driven rain is an important factor in its potential impact to building fabric. Projected changes in seasonal indices were also calculated, by summing I over all 20-year periods in the standard climatological seasons of winter (December to February) and summer (June to August) and are shown in Figure 17 and Figure 18 respectively. An increase in wind-driven rain is seen at all locations for southerly and westerly wall orientations in winter under both 2°C and 4°C of warming (Figure 17). Little change is projected for easterly directions. In contrast, a decrease in wind-driven rain is projected for summer (Figure 18) for all wall orientations. Large reductions are seen for westerly orientations at most locations; the exceptions are Kinloss and Wick. This contrasting pattern between summer and winter explains the lack of difference between periods in the annual I_A values. Spring (March to May) and August (September to November) were also investigated but exhibited little differences between the baseline and two future periods.

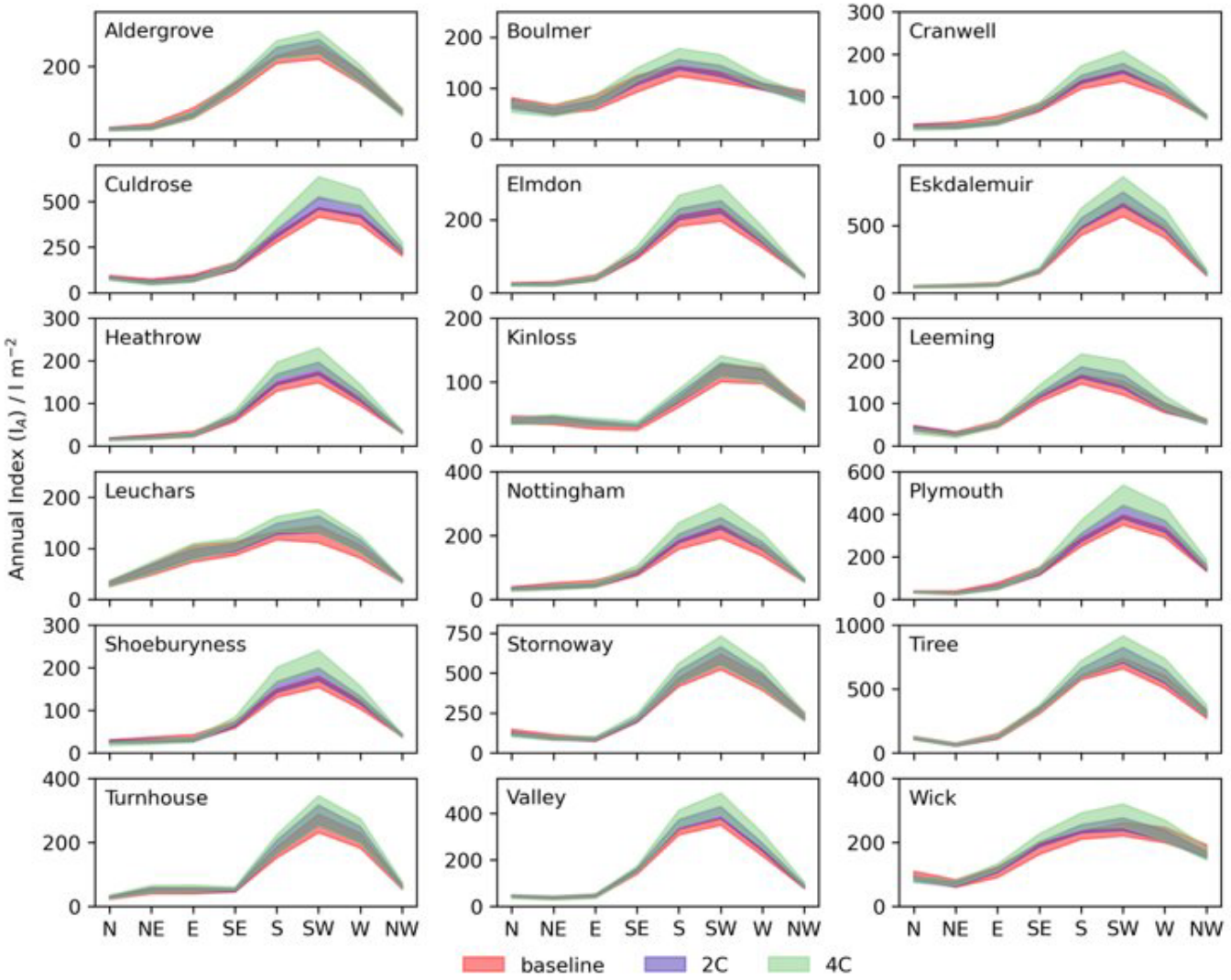

Figure 17. Projected values of the seasonal index (I_A) for winter (December to February) at the locations of the weather stations. Data are shown for the time periods corresponding to the baseline and times when global warming is 2°C and 4°C above pre-industrial levels. The shaded areas show the maximum and minimum values of the seasonal index across the UKCP18 CPM ensemble.

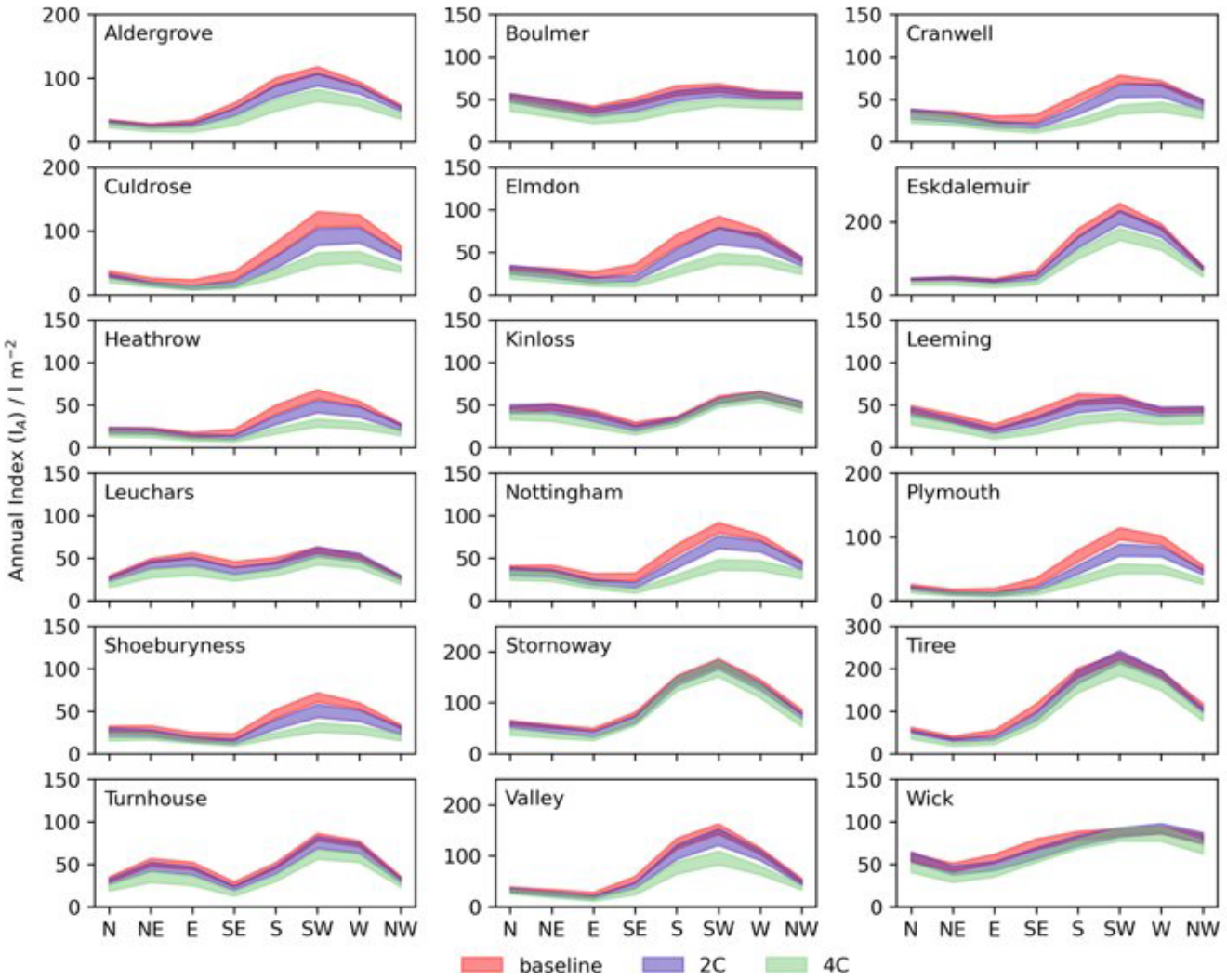

Figure 18. Projected values of the seasonal index (I_A) for summer (June to August) at the locations of the weather stations. Data are shown for the time periods corresponding to the baseline and times when global warming is 2°C and 4°C above pre-industrial levels. The shaded areas show the maximum and minimum values of the seasonal index across the UKCP18 CPM ensemble.

The percentage changes in the annual and seasonal indices at the weather stations are shown in Figure 19. The changes projected for annual, spring and autumn are centred at or close to zero for both levels of warming. Under 2°C warming, the projected changes for winter range from zero to +10%, whereas for summer they range from 0% to -20%. Larger changes are projected under the 4°C scenario. Wind-driven rain in winter is projected to increase by 10% to 25%, where in summer it could decrease between -10% and -45%. The annual and seasonal changes under the 4°C scenario are similar to those calculated by Orr et al. (2018) for 2070–2099. It should be noted that the changes shown in Figure 19 are for illustration only. The projected changes in other parts of the UK could be larger or smaller than those shown here.

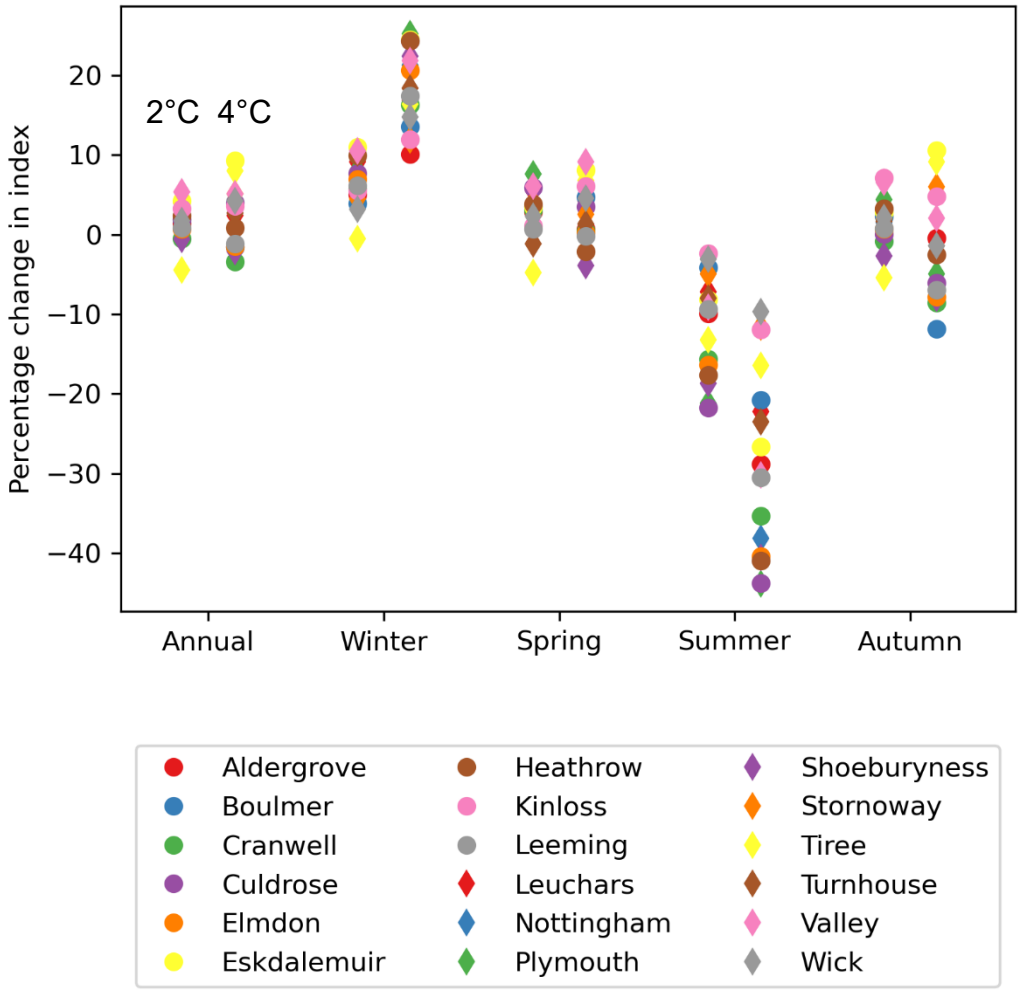

Figure 19. Percentage changes in the annual and seasonal wind-driven rain indices for the selected weather stations. For each season, two sets of changes are shown. The projected changes for the 2°C and 4°C scenarios are shown on the left and right respectively.

Changes in numbers of wet spells

Table 3 shows the numbers of wet spells (i.e., spells of wind-driven rain) in three different length ranges (less than 10 hours, 10 – 99 hours, and 100 hours or longer) for the three time periods (baseline (1981-2000), 2°C and 4°C of warming) calculated using CPM data at the location of each weather station. The numbers of short spells (less than 10 hours) increase with global warming at many stations, although little change or a small decrease is projected at stations on western coasts and in Scotland. A reduction in the numbers of long spells (100 hours or longer) is projected at all stations. The projected changes in the medium length spells (between 10 and 100 hours) are more mixed, with a maximum in numbers projected for 2°C of warming at some stations whereas a general decline in numbers of medium length wet spells is projected at others. This result suggests that, in the future, a greater proportion of wind-driven rain would occur in shorter spells. A similar conclusion was reached by Orr et al. (2018).

Table 3. Numbers of wet spells within three length ranges, for the baseline and two future periods corresponding to 2°C and 4°C of warming above pre-industrial levels. The ensemble mean and 95% confidence intervals are shown.

Station	Time Period	Short spells (less than 10 hours)	Medium spells (10 to 99 hours)	Long spells (100 hours or longer)
Aldergrove	baseline	90 ± 8	147 ± 10	182 ± 11
	2°C	96 ± 8	151 ± 9	177 ± 12
	4°C	98 ± 8	140 ± 10	157 ± 13
Boulmer	baseline	103 ± 5	167 ± 8	186 ± 10
	2°C	111 ± 5	165 ± 7	180 ± 11
	4°C	115 ± 6	158 ± 8	159 ± 11
Cranwell	baseline	116 ± 6	155 ± 6	163 ± 12
	2°C	120 ± 6	158 ± 5	153 ± 12
	4°C	121 ± 7	143 ± 6	132 ± 12
Culdrose	baseline	97 ± 8	143 ± 8	168 ± 11
	2°C	98 ± 8	143 ± 8	161 ± 12
	4°C	98 ± 8	131 ± 8	140 ± 12
Elmdon	baseline	111 ± 7	156 ± 7	161 ± 12
	2°C	115 ± 7	154 ± 6	151 ± 13
	4°C	118 ± 8	138 ± 6	128 ± 12
Eskdalemuir	baseline	76 ± 7	148 ± 11	186 ± 10
	2°C	81 ± 8	150 ± 11	181 ± 11
	4°C	80 ± 8	137 ± 11	162 ± 12
Heathrow	baseline	126 ± 7	154 ± 5	147 ± 12
	2°C	128 ± 7	154 ± 5	136 ± 13
	4°C	130 ± 8	134 ± 5	113 ± 11

Kinloss	baseline	98 ± 6	164 ± 9	187 ± 10
	2°C	98 ± 6	162 ± 9	185 ± 11
	4°C	99 ± 7	153 ± 10	169 ± 13
Leeming	baseline	117 ± 5	169 ± 6	179 ± 10
	2°C	119 ± 6	169 ± 6	169 ± 10
	4°C	125 ± 7	157 ± 7	147 ± 11
Leuchars	baseline	112 ± 5	167 ± 6	174 ± 11
	2°C	113 ± 6	167 ± 6	168 ± 12
	4°C	115 ± 6	156 ± 7	153 ± 13
Nottingham Watnall	baseline	110 ± 6	157 ± 7	166 ± 12
	2°C	112 ± 7	157 ± 6	156 ± 12
	4°C	114 ± 8	139 ± 7	135 ± 12
Plymouth	baseline	109 ± 8	147 ± 7	157 ± 13
	2°C	108 ± 8	145 ± 6	148 ± 12
	4°C	106 ± 8	128 ± 7	126 ± 12
Shoeburyness Landwick	baseline	133 ± 7	157 ± 5	148 ± 12
	2°C	136 ± 6	153 ± 4	136 ± 11
	4°C	135 ± 7	135 ± 6	114 ± 11
Stornoway Airport	baseline	61 ± 5	145 ± 11	203 ± 7
	2°C	65 ± 6	140 ± 12	198 ± 8
	4°C	62 ± 7	134 ± 13	182 ± 10
Tiree	baseline	71 ± 7	148 ± 11	194 ± 8
	2°C	73 ± 7	144 ± 11	191 ± 9
	4°C	72 ± 8	136 ± 13	174 ± 11

Turnhouse	baseline	102 ± 6	157 ± 8	174 ± 12
	2°C	104 ± 6	161 ± 7	168 ± 13
	4°C	103 ± 7	145 ± 8	152 ± 13
Valley	baseline	101 ± 8	151 ± 8	175 ± 11
	2°C	102 ± 8	153 ± 8	168 ± 11
	4°C	107 ± 9	141 ± 8	150 ± 12
Wick Airport	baseline	76 ± 5	153 ± 10	204 ± 8
	2°C	79 ± 6	149 ± 10	202 ± 9
	4°C	77 ± 7	145 ± 12	186 ± 11

Changes in magnitudes of 1 in 3 year spells

The magnitudes of 1 in 3 year wind-driven rain spells (i.e., those spells with a return period of 3 years) were calculated for periods corresponding to 2°C and 4°C of warming. Data from all ensemble members were pooled together for each time period. The magnitudes of the 1 in 3 years events were calculated using the pooled data. Maps showing the percentage changes in the 1 in 3 year spells are shown in Figure 20 for 2°C and Figure 21 for 4°C of warming.

Under 2°C warming, the magnitudes of 1 in 3 years spells are projected to decrease for all wall orientations. Reductions as high as 50% are projected, although most changes are smaller. The least change is projected for south and south-west facing walls. For 4°C warming, the changes are more polarised. Larger reductions in 1 in 3 years spells are projected for all wall orientations with a north or easterly component. In contrast, increase in 1 in 3 year spells are projected over England and Wales for south and west-facing walls, especially over western coasts.

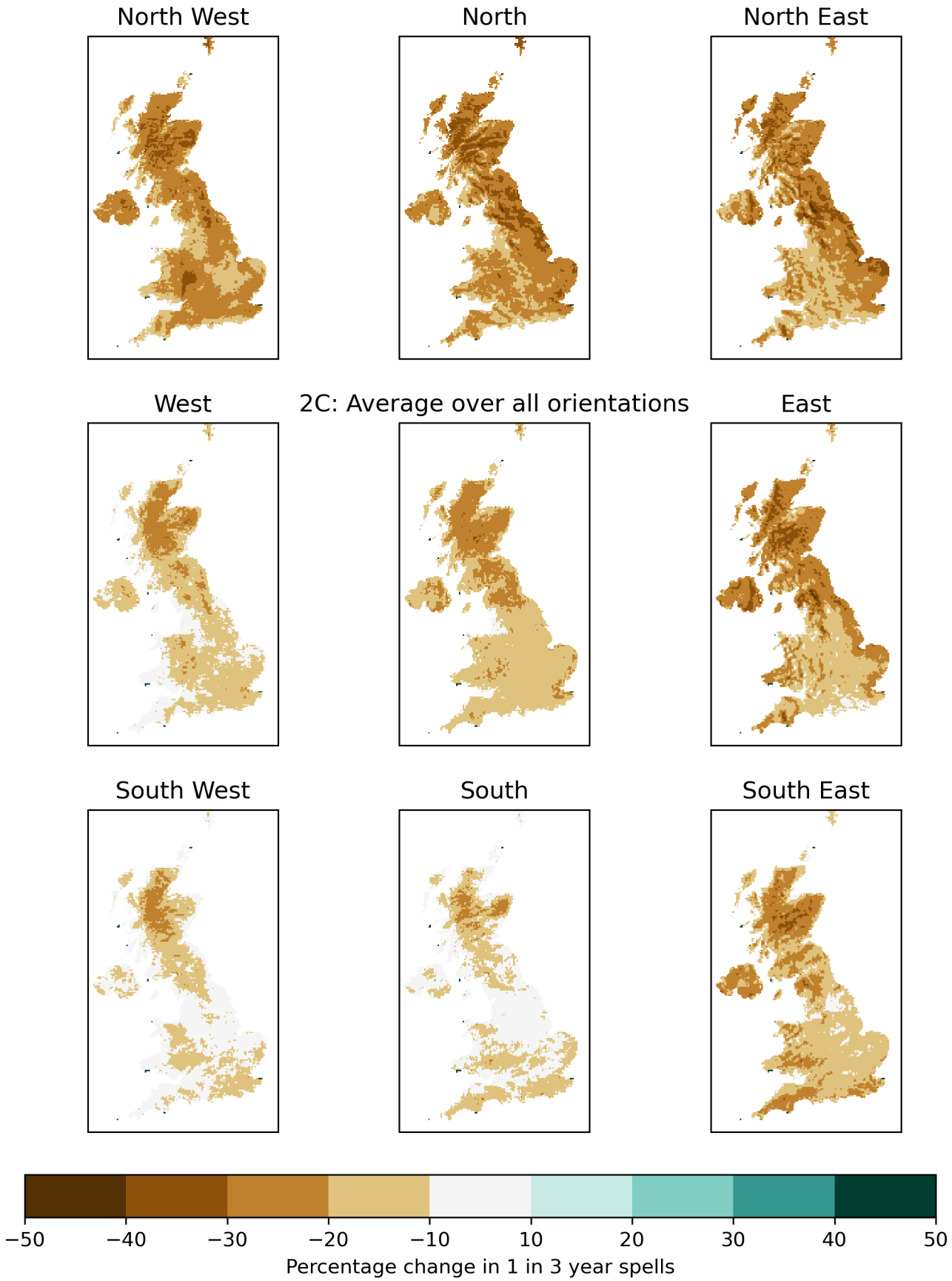

Figure 20. Maps showing the percentage changes in the magnitudes of 1 in 3 year wind-driven rain spells for 2°C of warming for each wall orientation.

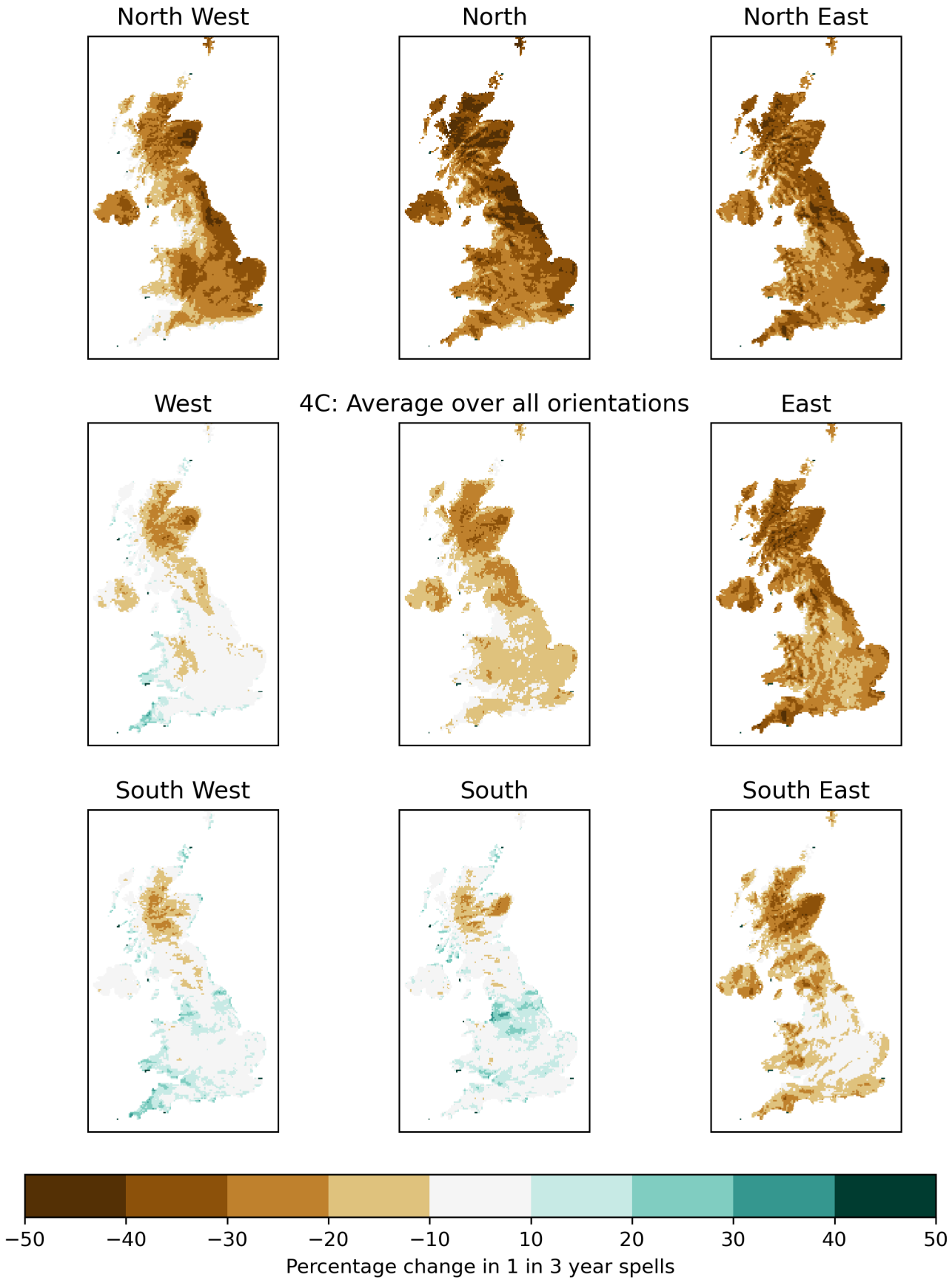

Figure 21. Maps showing the percentage changes in the magnitudes of 1 in 3 year wind-driven rain spells for 4°C of warming for each wall orientation.

Discussion

The wind-driven rain metric used in this study is an industry-standard that appears to have been derived from limited observations of rain droplet size distributions and raindrop terminal velocities (Lacy, 1977; Orr et al., 2018). The wind-driven rain metric is not suitable for mountainous areas with sheer cliffs or deep gorges, areas where severe convective storms contribute more than 25% of annual rainfall amounts, or areas and periods where snow or hail make up significant portions of precipitation (Orr and Viles, 2018). The validity of the use of the cosine of the angle between the wind direction and the wall orientation has also been called into question (Blocken and Carmeliet, 2006). However, the use of the cosine remains the current standard for incorporating wall orientation into evaluations of wind-driven rain exposure (Orr et al., 2018).

Alternative approaches for quantifying wind-driven rain have been used in other studies. Lacy (1977) produced maps of the UK with contours of an omnidirectional driving rain index with units of $m^2 s^{-1}$. A series of tables accompanied the map which listed corrected driving rain indices for different types of location and building heights. Prior (1985) produced maps of annual wind-driven rain amounts (also in $m^2 s^{-1}$) for a range of different wall orientations. Tables were provided listing multiplicative factors for topography and roughness, which modify the mapped values according to building height and terrain type. This approach was used in BS:8104 (BSI, 1992). Rydock et al. (2005) classified 12 hour periods as moistening, drying or neutral based on the wind speed, direction and rainfall amounts. The average wind direction during the 12-hour period was calculated; wind-driven rain was said to strike a wall if the average direction was within 60° of the perpendicular to a given wall orientation. Ra (2018) sorted hourly data from weather stations in South Korea into 16 different wind directions and calculated annual wind-driven rain indices for each direction using the same equation as Lacy and Shellard (1962) (see equation 1).

Prior (1985) included a figure showing the collection efficiency of wind-driven rain on a wall as a function of the product of the wind speed and angle between the wind direction and wall orientation, i.e., collection efficiency is proportional to $v \times \cos(d - \theta)$ where v is wind speed, d is wind direction, and θ is wall orientation (see equation 3). However, this figure was based on very limited data. Xiao et al. (2021) calculated the wind-driven rain load on buildings by multiplying the annual index, IA (equations 4 and 5) by four factors which represent the local terrain roughness, topography, obstruction by other buildings and the properties of the walls. Gholamalipour et al. (2022) summarised other wind-driven rain equations that include multiplicative factors which attempt to quantify the exposure of a building and how readily rain would deposit to its surface. These methods which estimate the actual rain load on walls are currently not set out in any standard. A comparison of results using different wind-driven rain metrics would be the subject of a separate study.

This study has focused on the airfield index, which is the amount of wind-driven rain in the absence of any obstructions. A modified dataset could be created by multiplying the airfield

indices by some of the factors relating to building heights and terrain types from the British Standard BS 8104:1992.

The underlying climate data were produced with variants of a single climate model. Consequently, the range of projected changes in wind-driven rain do not include a consideration of model structural uncertainty. Other climate models might project different changes in wind-driven rain under a warming climate. For example, the UKCP18 global models project larger reductions in summer precipitation over the UK than many other CMIP5 models (Murphy et al., 2018). The UKCP18 models also project a much larger increase in the number of winter storms that cross the UK than the CMIP5 models. These results suggest that the range of changes in wind-driven rain projected by other models could be smaller than those shown in Figure 17 to Figure 19.

This study used data at a resolution of 5 km, from which only daily mean wind directions could be calculated. The use of daily mean directions will introduce biases into the results, with southeasterly directions seemingly most affected. However, even hourly mean wind directions might not reflect the true wind direction when rain was falling (Prior, 1985). The underlying climate data were produced by a model with 2.2 km resolution. Hourly wind direction data are also available on the 2.2 km grid. One future improvement would be to aggregate the hourly wind direction data to the 5 km grid.

The modelled daily mean wind speeds were bias-corrected assuming they follow a Weibull distribution, and then used to adjust the hourly wind speeds. A comparison of five different bias-correction methods for wind speeds by Li et al. (2019) indicated that the Weibull method performed the best. Tests showed that the wind speeds in the CPM could be represented well by a Weibull distribution. This bias-correction approach assumes the statistical relationship between the model and observations does not change over time, which may not be the case. Other bias-correction methods could have been used, but a comparison of results using different methods is beyond the scope of the current project.

Conclusions

A high resolution gridded wind-driven rain dataset has been created for the UK using hourly climate data from the UKCP18 climate projections. The airfield metric was calculated, which quantifies wind-driven rain in the absence of any obstructions. The airfield and other metrics calculated from the modelled wind-driven rain data compared well with those calculated from data recorded at weather stations located around the UK. The UKCP18 projections include climate data from an ensemble of 12 versions of the climate model, allowing some of the uncertainty in climate projections to be included in any assessments of wind-driven rain.

Unlike existing datasets, wind-driven rain has been calculated for a baseline period (1981-2000) and two future time periods corresponding to 2°C and 4°C of warming above pre-industrial levels. Wind-driven rain is projected to increase in winter but decrease in summer under a warming climate. Projected changes in annual averages of wind-driven rain were small. The projected changes in wind-driven rain have a strong directional component; reductions in wind-driven rain were projected for north- and east-facing walls but an increase was projected for south- and west-facing walls. The largest increases in wind-driven rain were projected for west-facing coastal areas and higher altitude locations.

Extreme wind-driven rain events have not been considered here. It could be of interest to locate extreme events in the modelled data and compare them with known events. The impacts of climate change on these extreme events could be smaller or larger than impacts on average changes in wind-driven rain.

The wind-driven metric used in this study appears to have been derived from limited measurements of rain droplet sizes and raindrop terminal velocities. One improvement would be to locate information on raindrop sizes associated with different rainfall intensities and modify the wind-driven rain metric accordingly. Wind-driven rain would be then quantified using a metric tailored to a given rainfall intensity, which more closely relates to the way wind driven rain can damage building fabric.

At the time of writing, the Met Office is downscaling global climate projections produced by other modelling centres to produce additional high-resolution climate information for the UK. Wind-driven rain could be quantified from these new simulations and compared with wind-driven rain calculated from the UKCP18 projections. The size and sign of projected changes in wind-driven rain in a warmer climate could also be compared.

References

Blischke W.R., Scheuer E.M. (1986). Tabular aids for fitting Weibull moment estimates. Naval Research Logistics Quarterly, 33, 145-153, doi:10.1002/nav.3800330113

Blocken B., Carmeliet J. (2004). A review of wind-driven rain research in building science. Journal of Wind Engineering & Industrial Aerodynamics, 92, 1079–1130, doi:10.1016/j.jweia.2004.06.003

Blocken B., Carmeliet J. (2006). On the validity of the cosine projection in wind-driven rain calculations on buildings. Building and Environment, 41, 1182-1189, https://doi.org/10.1016/j.buildenv.2005.05.002

Bloomfield H.C., Brayshaw D.J., Charlton-Perez A.J. (2019). Characterizing the winter meteorological drivers of the European electricity system using targeted circulation types. Meteorological Applications, 27, e1858, https://doi.org/10.1002/met.1858.

Boogaard H., Schubert J., De Wit A., Lazebnik J., Hutjes R., Van der Grijn G. (2020). Agrometeorological indicators from 1979 to present derived from reanalysis. Copernicus Climate Change Service (C3S) Climate Data Store (CDS). doi:10.24381/cds.6c68c9bb (Accessed on 24-May-2023)

Brimblecombe P., Richards J. (2023). Temporal resolution of climate pressures on façades in Oxford 1815–2021. Theoretical and Applied Climatology, 153, 561–572. https://doi.org/10.1007/s00704-023-04498-x

BSI, 1992. BS 8104:1992 – Code of Practice for Assessing Exposure of Walls to Wind-driven Rain, Standard. British Standards Institution.

Gaylarde C.C. (2020). Influence of Environment on Microbial Colonization of Historic Stone Buildings with Emphasis on Cyanobacteria. Heritage, 3, 1469–1482. https://doi.org/10.3390/HERITAGE3040081

Gholamalipour P., Ge H., Stathopoulos T. (2022). Wind-driven rain (WDR) loading on building facades: A state-of-the-art review. Building and Environment. 221, 109314, doi:10.1016/j.buildenv.2022.109314.

Hand W.H., Fox N.I., Collier C.G. (2004). A study of twentieth-century extreme rainfall events in the United Kingdom with implications for forecasting. Meteorological Applications, 11, 15-31, https://doi.org/10.1017/S1350482703001117

Hanlon H.M., Bernie D., Carigi G., Lowe J.A. (2021). Future changes to high impact weather in the UK. Climatic Change, 166, 50, https://doi.org/10.1007/s10584-021-03100-5

Hersbach H. et al. (2020). The ERA5 global reanalysis. Quarterly Journal of the Royal Meteorological Society, 146A, 1999-2049, https://doi.org/10.1002/qj.3803

HM Government (2004). The Buildings Regulations 2004: Site preparation and resistance to contaminants and moisture. Approved Document C (with 2010 and 2013 amendments).

Hollis D., McCarthy M., Kendon M., Legg T., Simpson I. (2019). HadUK-grid – a new UK dataset of gridded climate observations. Geoscience Data Journal, 6, 151–159, https://doi.org/10.1002/gdj3.78

International Organization for Standardization, 2009. Hygrothermal Performance of Buildings – Calculation and Pre-sensation of Climatic Data – Part 3: Calculation of a Driving Rain Index for Vertical Surfaces from Hourly Wind and Rain Data.

Jones P., Harpham C., Kilsby C., Glenis V., Burton A. (2010). UK Climate Projections science report: Projections of future daily climate for the UK from the Weather Generator. https://core.ac.uk/download/pdf/299302528.pdf

Kelly M., Troen I., Jørgensen H.E. (2014). Weibull-k Revisited: “Tall” Profiles and Height Variation of Wind Statistics. Boundary-Layer Meteorology, 152, 107–124, https://doi.org/10.1007/s10546-014-9915-5

Kendon E.J., Fischer E.M., Short C.J. (2023a). Variability conceals emerging trend in 100yr projections of UK local hourly rainfall extremes. Nature Communications, 14, 1133, https://doi.org/10.1038/s41467-023-36499-9

Kendon L. et al. (2023b). UK Climate Projections: UKCP Local (2.2km) Transient Projections. Met Office Hadley Centre, Exeter, UK.

Kovats S., Brisley R. (2021). Health, communities and the built environment. In: The Third UK Climate Change Risk Assessment Technical Report [Betts, R.A., Haward, A.B., Pearson, K.V. (eds.)]. Prepared for the Climate Change Committee, London, UK. https://www.ukclimaterisk.org/wp-content/uploads/2021/06/CCRA3-Chapter-5-FINAL.pdf

Lacy R.E., Shellard H.C. (1962). An index of driving rain. Meteorological Magazine, Vol. 91, No. 1080, 177-184.

Lacy R.E. (1976). Driving-rain index. Annual mean driving-rain index in the United Kingdom with proposed revised rules for assessing local exposure. Paper No. 5/72, Building Research Establishment, UK.

Lacy R.E. (1977). Climate and Building in Britain. Her Majesty’s Stationery Office, London.

Lea D.A., Helvey R.A. (1971). A Directional Bias in Wind Roses Due to Mixed Compass Formats. Journal of Applied Meteorology, 10,1037-1039, https://doi.org/10.1175/1520-0450(1971)010<1037:ADBIWR>2.0.CO;2

Lewis E., Quinn N., Blenkinsop S., Fowler H.J., Freer J., Tanguy M., Hitt O., Coxon G., Bates P., Woods R. (2018). A rule based quality control method for hourly rainfall data and a 1 km resolution gridded hourly rainfall dataset for Great Britain: CEH-GEAR1hr. Journal of Hydrology, 564, 930-943, https://doi.org/10.1016/j.jhydrol.2018.07.034

Li D. Feng J., Xu Z., Yin B., Shi H., Qi J. (2019). Statistical Bias Correction for Simulated Wind Speeds Over CORDEX-East Asia. Earth and Space Science, 6, 200-211, https://doi.org/10.1029/2018EA000493

Lowe J.A. et al. (2018). UKCP18 Science Overview Report. Met Office Hadley Centre, Exeter, UK.

Met Office (2019): Met Office MIDAS Open: UK Land Surface Stations Data (1853-current). Centre for Environmental Data Analysis, accessed 03 July 2023. http://catalogue.ceda.ac.uk/uuid/dbd451271eb04662beade68da43546e1

Murphy J.M. et al. (2018). UKCP18 Land Projections: Science Report. Met Office Hadley Centre, Exeter, UK.

Ordnance Survey (2020). A guide to coordinate systems in Great Britain. https://www.ordnancesurvey.co.uk/documents/resources/guide-coordinate-systems-great-britain.pdf

Orr S.A., Viles H. (2018). Characterisation of building exposure to wind-driven rain in the UK and evaluation of current standards. Journal of Wind Engineering & Industrial Aerodynamics, 180, 88-97, doi:10.1016/j.jweia.2018.07.013

Orr S.A., Young M., Stelfox D., Curran J., Viles H. (2018). Wind-driven rain and future risk to built heritage in the United Kingdom: Novel metrics for characterising rain spells. Science of the Total Environment, 640-641C, 1098–1111, doi:10.1016/j.scitotenv.2018.05.354

Pope J.O., Brown K., Fung F., Hanlon H., Neal R., Palin E.J., Reid A. (2022). Investigation of future climate change over the British Isles using weather patterns. Climate Dynamics, 58, 2405–2419, https://doi.org/10.1007/s00382-021-06031-0

Prior M.J. (1985). Directional driving rain indices for the United Kingdom — computation and mapping. Building Research Establishment Report, Garston, UK.

Ra J.B. (2018). Determination of driving rain index by using hourly weather data for developing a good design of wooden buildings. Journal of Korean Wood Science and Technology, 46, 627-636, https://doi.org/10.5658/WOOD.2018.46.6.627.

Richards J., Brimblecombe P. (2022). Moisture as a Driver of Long-Term Threats to Timber Heritage. Part I: Changing Heritage Climatology. Heritage 5:1929–1946. https://doi.org/10.3390/HERITAGE5030100

Ruedrich J., Kirchner D., Siegesmund S. (2011). Physical weathering of building stones induced by freeze–thaw action: a laboratory long-term study. Environmental Earth Sciences, 63, 1573–1586, https://doi.org/10.1007/s12665-010-0826-6

Rydock J.P., Lisø K.R., Førland E.J., Oswaldová K., Thue J.V. (2005). A driving rain exposure index for Norway. Building and Environment, 40, 1450–1458, https://doi.org/10.1016/j.buildenv.2004.11.018

Souri F., Ge H., Stathopoulos, T. (2021). Wind-driven rain on buildings: Accuracy of the ISO semi-empirical model. Journal of Wind Engineering & Industrial Aerodynamics, 212, 10460, https://doi.org/10.1016/j.jweia.2021.104606

Watkiss P., Betts R.A. (2021). Method. In: The Third UK Climate Change Risk Assessment Technical Report [Betts, R.A., Haward, A.B. and Pearson, K.V. (eds.)]. Prepared for the Climate Change Committee, London.

Xiao Z., Lacasse MA, Dragomirescu E. (2021). An analysis of historical wind-driven rain loads for selected Canadian cities. Journal of Wind Engineering & Industrial Aerodynamics, 213, 104611, https://doi.org/10.1016/j.jweia.2021.104611

Zeng Z., Ziegler A.D., Searchinger T., Yang L., Chen A., Ju K., Piao S., Li L.Z.X., Ciais P., Chen D., Liu J., Azorin-Molina C., Chappell A., Medvigy D., Wood E.F. (2019). A reversal in global terrestrial stilling and its implications for wind energy production. Nature Climate Change, 9, 979‑985. https://doi.org/10.1038/s41558-019-0622-6

Appendix

A1. Bias-correction of daily mean wind speeds

A quantile mapping approach is used to bias-correct daily mean wind speeds. The long-term second moment of wind speed $\langle U^2 \rangle$ is comprised of independent first- and second-order contributions (Kelly et al., 2014):

$$\langle U^2 \rangle = \langle U \rangle^2 + \sigma_U^2$$

A Weibull distribution is fitted to the wind speeds for a given month using the method of moments. The nth moment of the wind speed (which closely follows a Weibull distribution) is given by:

$$\langle U^n(z) \rangle = A^n \Gamma(1 + n/k)$$

where Γ is the gamma function, U is the wind speed at height z, A is the scale parameter and k is the Weibull shape parameter. If the second moment (n = 2) is divided by the square of the first moment (n = 1), and the top equation is used to substitute the term $\langle U^2 \rangle$, the scale parameter can be eliminated and the following equation is obtained (Blischke and Scheuer, 1986; Kelly et al., 2014):

$$\frac{\sigma_U^2}{\langle U \rangle^2} = \frac{\Gamma(1 + 2/k)}{\Gamma^2(1 + 1/k)} - 1$$

where $\langle U \rangle^2$ and σ_U^2 are set equal to the square of the sample mean ($\overline{U}$) and variance respectively. This equation can be solved numerically to find k. The scale parameter A is then found by rearranging the first moment:

$$A = \frac{\overline{U}}{\Gamma(1 + 1/k)}$$

The Weibull distribution is fitted to both the modelled and observed (here, AgERA5) wind speeds. The modelled wind speeds are then bias-corrected by assigning the speeds from AgERA5 which have the same quantiles, using equations from Li et al. (2019).

Table A1. Locations of 18 weather stations used to evaluate the modelled data. Hourly climate data for 1981-2000 were available from these stations.

Name	Northing	Easting	Altitude (m)
Aldergrove	536008	126357	63
Boulmer	614178	425338	23
Cranwell	349260	500451	63
Culdrose	25560	167096	76
Elmdon	283900	417600	96
Eskdalemuir	602638	323498	236
Heathrow	176724	507693	25
Kinloss	862804	306774	5
Leeming	489141	430491	33
Leuchars	720895	346862	10
Nottingham Watnall	345627	450342	117
Plymouth Mountbatten	52710	249216	50
Shoeburyness Landwick	187772	596079	2
Stornoway Airport	933097	146438	15
Tiree	744871	99782	9
Turnhouse	673900	315900	35
Valley	375849	230885	10
Wick Airport	952230	336490	36

Table A2. Twenty year periods when global warming reaches 2°C and 4°C above pre-industrial levels in the UKCP18 global climate projections under the RCP8.5 scenario. The pre-industrial period is defined as 1850-1900.

Ensemble Member	2°C	4°C
1	2019-2038	2053-2072
4	2017-2036	2050-2069
5	2022-2041	2056-2075
6	2019-2038	2054-2073
7	2020-2039	2054-2073
8	2022-2041	2059-2078
9	2017-2036	2047-2066
10	2021-2040	2057-2076
11	2018-2037	2054-2073
12	2024-2043	2057-2076
13	2018-2037	2053-2072
15	2022-2041	2058-2077

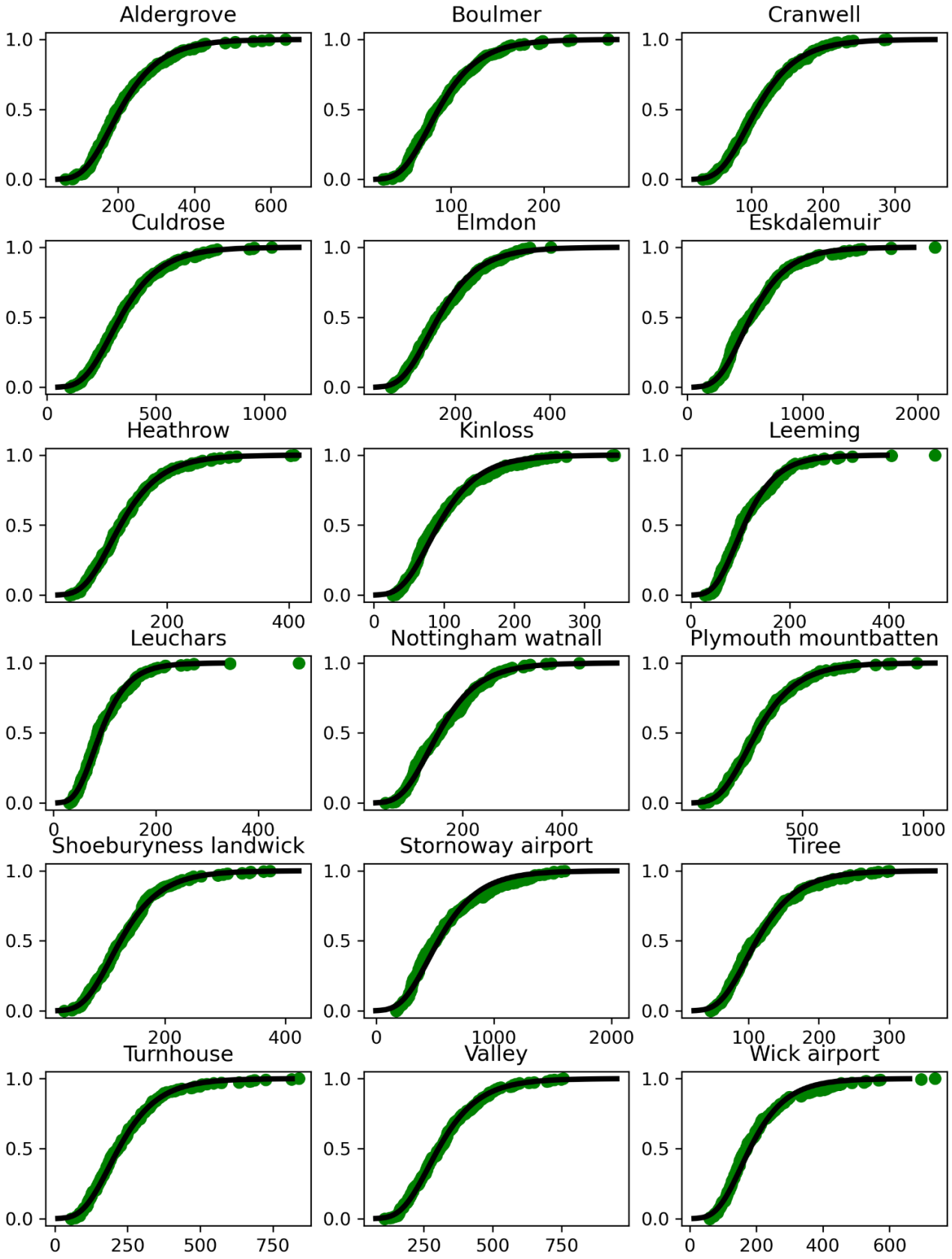

Figure A1: Fit of Gumbel distribution to annual maxima of wind-driven rain spells for south-west facing walls. Green symbols indicate annual maxima of wind-driven rain spells in the CPM data for all ensemble members. The solid black line shows the cumulative distribution function of the fitted Gumbel distribution. The x-axes show the magnitudes of the annual maximum wind-driven rain spells.

This publication is available from: www.gov.uk/desnz

If you need a version of this document in a more accessible format, please email alt.formats@beis.gov.uk. Please tell us what format you need. It will help us if you say what assistive technology you use.